10

Sample Application of 'Active' DOAS with Artificial Light Sources

Over the past 25 years, active DOAS measurements have been made for a multitude of purposes. From the initial studies of the atmospheric composition in the mid 1970s, a wide variety of designs and applications in the open atmosphere, as well as in the laboratory, have been developed.

For instance, broadband lasers were used as a light source (Rothe et al., 1974; Perner et al., 1976; Perner et al., 1991; Amerding et al., 1991; Dorn et al., 1993, 1996, 1998; Brauers et al., 1996, 1999; Brandenburger et al., 1998). However, the majority of the designs rely on arc-lamps as light sources (e.g. Bonafe et al., 1976; Kuznetzov and Nigmatullina, 1977; Noxon et al., 1978, 1980; Platt, 1977; Evangelisti et al., 1978; Platt et al., 1979; Platt and Perner, 1980, 1983; Johnston and McKenzie, 1984; Dorn and Platt, 1986; Edner et al., 1986, 1990, 1992, 1993a,b, 1994a; Axelsson et al., 1990a,b, 1995; Axelsson and Lauber, 1992; Amerding et al., 1991; Wagner, 1990; Hallstadius et al., 1991; Galle et al., 1991; Biermann et al., 1991; Stevens and Vossler, 1991; Gall et al., 1991; Fayt et al., 1992; Plane and Nien, 1992; Vandaele et al., 1992; Hausmann et al., 1992, 1997; Stevens et al., 1993; Hausmann and Platt, 1994; Martini et al., 1994; Plane and Smith, 1995; Evangelisti et al., 1995; Heintz et al., 1996; Harder et al., 1997; Flentje et al., 1997; Lamp et al., 1998; Reisinger et al., 1998; Russwurm, 1999; Allan et al., 1999, 2000; Hebestreit et al., 1999; Alicke, 2000; Gölz et al., 2001; Kim and Kim, 2001; Geyer et al., 1999, 2001a,b,c, 2002, 2003; Matveev et al., 2001; Volkamer et al., 2001; Alicke et al., 2002; Veitel et al., 2002; Lee et al., 2002; Yu et al., 2004; Saiz-Lopez et al., 2004a,b; Lee et al., 2005; Zingler and Platt, 2005). In addition there is a small number of recent studies using artificial 'lights of opportunity' to perform DOAS measurements (Yoshii et al., 2003; Fuqi et al., 2005). It is impossible to review the entire breadth of DOAS studies over the past three decades. However, it is instructive to consider examples for some of the most valuable uses of active DOAS. The intention of this chapter is to provide an overview of the abilities DOAS offers to research in atmospheric chemistry and physics. We hope that this overview will inspire the development of even more applications in the future.

U. Platt and J. Stutz, *Sample Application of 'Active' DOAS with Artificial Light Sources*. In: U. Platt and J. Stutz, Differential Optical Absorption Spectroscopy, Physics of Earth and Space Environments, pp. 379–427 (2008)
DOI 10.1007/978-3-540-75776-4_10

10.1 Air Pollution Studies and Monitoring Applications

Motivated by the desire to understand and mitigate air quality problems in urban areas such as Los Angeles, one of the earliest uses for active DOAS was the investigation of the processes leading to the formation of urban air pollution. Today, DOAS is used as a tool to monitor air quality and also as a benchmark for other techniques. DOAS is an Environmental Protection Agency (EPA) approved method to monitor primary pollutants such as O_3, NO_2, and SO_2. In addition, the Association of German Engineers (Verein Deutscher Ingenieure, VDI) issued a draft guideline for the testing of DOAS instruments for air pollution monitoring (VDI, 2005). A number of commercial DOAS instruments are available today. All these instruments work according to the principles described in earlier chapters. The advantages of DOAS for monitoring purposes are high accuracy and the ability to measure all three pollutants simultaneously.

In the following section, we will concentrate on state-of-the-art research applications to illustrate the abilities that DOAS has to offer today's research community.

10.1.1 Measurement of Urban Pollutants

The measurement of pollutants is an important undertaking, both for air pollution-related research and the monitoring of air quality.

Ozone, *nitrogen dioxide*, and *sulphur dioxide* are some of the most important species connected to air pollution. SO_2 and NO_2 (in the form of NO which is rapidly converted to NO_2; see Chap. 2) are released from combustion sources. Ozone is formed throughout the day by photochemical processes, and is the main component of the so-called Los Angeles Smog (see Chap. 2). All three species are regulated in most industrialized countries (e.g. by the US Environmental Protection Agency), and considerable effort is put into their continuous measurement for air quality monitoring.

Ozone, NO_2, and SO_2 are, in most cases, the strongest absorbers in DOAS spectra acquired in polluted areas. These three trace gases are thus the most commonly measured species in active DOAS applications. Figure 10.1 shows an example of an analysis of O_3, NO_2, and SO_2 and in addition CH_2O in the UV made in Heidelberg, Germany in 1994 by a long-path DOAS instrument, such as those described in Chap. 7. The figure illustrates again how the analysis procedure outlined in Chap. 8 is used to separate the different absorption structures in an atmospheric absorption spectrum. The wavelength range displayed in Fig. 10.1 is typically chosen for the detection of O_3, SO_2, and HCHO in long-path DOAS applications. An example of the measurement of NO_2 was already given in Chap. 8.

Figures 10.2 and 10.3 show examples of measured time series of O_3, NO_2, SO_2, and a number of other trace gases during field experiments in Milan,

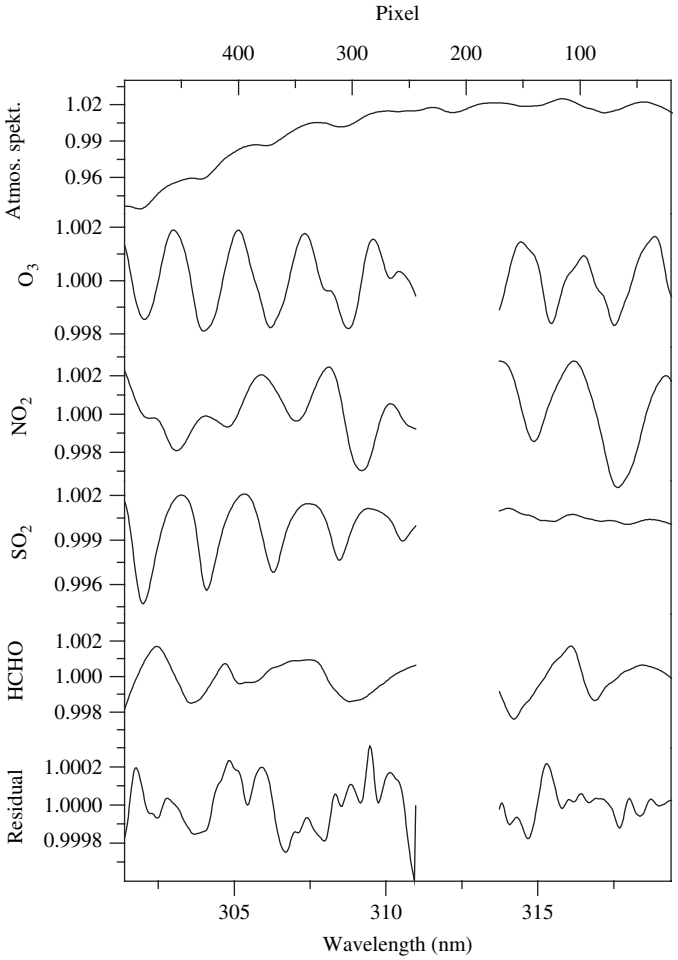

Fig. 10.1. Example of a spectral analysis of O_3, NO_2, SO_2, and HCHO in the polluted air of Heidelberg. The absorptions identified in the atmospheric spectrum (*top trace*) were: O_3, 21.1 ± 0.5 ppb; SO_2, 0.64 ± 0.01 ppb; and HCHO, 3.7 ± 0.1 ppb. The NO_2 mixing ratio was not determined since this wavelength interval is not optimal for its analysis. The missing area around 312 nm was excluded from the analysis procedure

Italy, and Houston, USA, respectively. The goal of both, the Pianura Padania Produzione di Ozono (Po-Valley Ozone Production, PIPAPO) study in Milan and the Texas Air Quality Study (TEXAQS) in Houston, was to investigate the formation of ozone and particles in the polluted environment of these cities.

The measurements in Milan were made with a long-path DOAS instrument that employed retro-reflectors to fold the light path once. This instrument

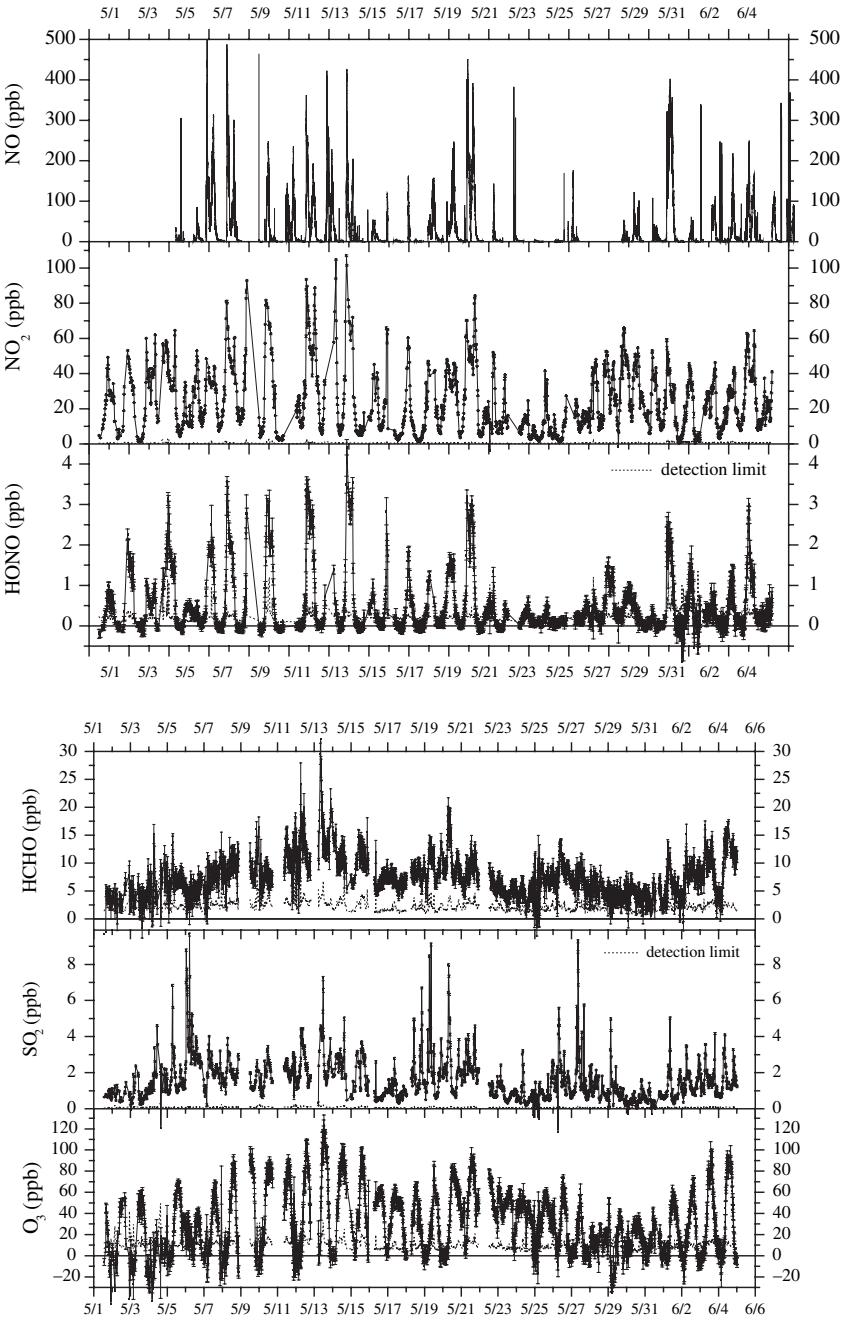

Fig. 10.2. Time series of O_3, NO_2, SO_2 HCHO, and HONO mixing ratios measured during the PIPAPO study in Milan, Italy. In addition, NO (top trace) was measured by chemoluminescence (from Alicke et al., 2002, Copyright by American Geophysical Union (AGU), reproduced by permission of AGU)

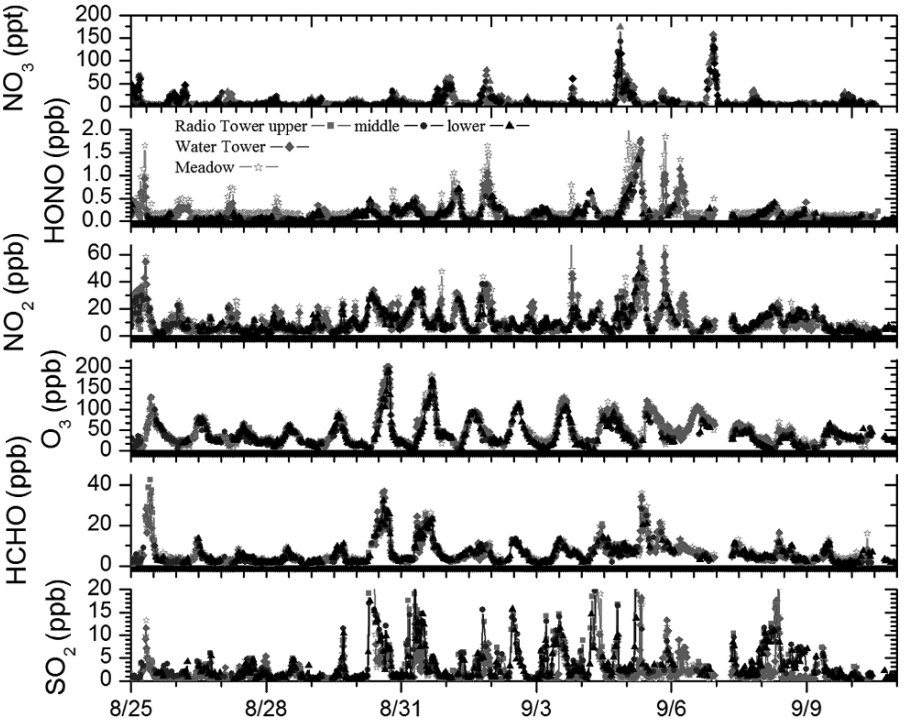

Fig. 10.3. O_3, NO_2, and SO_2, HONO, and NO_3 mixing ratios during the Texas Air Quality Study (TEXAQS) in summer 2000.The measurements in Houston, Texas (USA) were performed with two long-path DOAS instruments on five different light paths. A more detailed description of the set-up is given in Stutz, et al., (2004b)

was set up about 8 km north of the city centre of Milan at a small airport. The instrument could measure alternating on three light paths of different elevation (Fig. 10.6). Only the data from the upper light path are shown in Fig. 10.2. The mixing ratios of ozone in Milan show strong diurnal variations, with low levels at night when emission of NO converts O_3 to NO_2, and high levels after noon when ozone is photolytically formed (see Chap. 2). Mixing ratios of ozone exceeded 100 ppb on several occasions. Nitrogen dioxide shows a diurnal variation opposite to O_3, with high values at night and low values during the day. The NO_2 mixing ratios reached up to 100 ppb, showing that Milan is heavily polluted. The NO data, measured by a chemiluminescence instrument (see Chap. 5), also show extremely high mixing ratios. While the O_3 and NO_2 data are closely related to each other, the SO_2 data in Milan behaves quite differently. This can be explained by the different sources and chemistry of SO_2 which shows a higher short-term variability. Levels of SO_2 reached up to 8 ppb.

The observations in Houston (Fig. 10.3) were made using two DOAS instruments measuring on five different light paths (Fig. 10.15). A discussion of this set-up will be given in Sect. 10.1.2. The instruments were located 8 km south-east of downtown Houston, close to an industrial area with a large number of refineries. In general, the behaviour of O_3 and NO_2 is similar to that in Milan, and is typical for a polluted urban area. The levels of NO_2 are lower in Houston. However, ozone reached mixing ratios above 200 ppb on two occasions. SO_2 levels were also higher in Houston than in Milan, most likely due to emissions from the nearby refineries.

The time series from these two field experiments (Figs. 10.2 and 10.3) illustrate the ability of modern long-path DOAS instruments to continuously measure O_3, NO_2, and SO_2 at a time resolution of 5–15 min. The detection limits reached during these two campaigns are shown in Tables 10.1 and 10.2. One will notice that the detection limits vary with the light path length. This is caused by the presence of residual structures in the spectra of both experiments (see Chap. 8). The detection limits in Tables 10.1 and 10.2 give an indication of the performance of modern DOAS instruments.

Formaldehyde plays an important role in the chemistry of the troposphere. It is formed in the oxidation of most hydrocarbons, and also directly emitted from combustion sources. The photolysis of HCHO forms HO_2 radicals, which in the presence of NO are rapidly converted into OH. HCHO is thus an important HO_X precursor. DOAS measurements for the PIPAPO and TEXAQS field experiments are shown in Figs. 10.2 and 10.3. Typical levels in polluted urban areas are ~ 10 ppb. Only in heavily polluted environments with a fast photochemistry, such as Houston, are higher HCHO levels observed. The HCHO levels in Houston (Fig. 10.3) roughly follow the O_3 mixing ratios. This

Table 10.1. Overview of the species measured in Milan, Italy and the observed mixing ratios (adapted from Alicke et al., 2002)

Species	Wavelength window (nm)	Absorption cross-section	Maximum mixing ratio (ppb/date)	Detection limit (ppb)
HONO	375–336	(Stutz et al., 2000)	4.4 ± 0.2, 13.5.98 21:25	0.2
NO_2	375–336	(Harder et al., 1997)	115.2 ± 0.6, 13.5.98 21:08	0.6
NO	–		480, 7.5.98 21:30	0.25
SO_2	322–303	(Vandaele et al., 1994)	9.1 ± 0.22, 19.5.98 8:47	0.18
O_3	322–303	(Bass and Paur, 1985)	123 ± 9, 13.5.98 12:37	8.5
HCHO	322–303	(Cantrell et al., 1990)	33.6 ± 1.8, 13.5.98 8:32	1.6

The distance between telescope and retro-reflectors was 1.25 km.
*All times GMT (local – 2 h)

Table 10.2. Summary of data coverage, average and best detection limits for the DOAS results in Houston, Texas (USA), see details in Stutz et al., 2004b

	Lightpath 'meadow'	Lightpath 'water tower'	Lightpaths 'radio tower'
Distance (km)	0.75	1.9	6.1
Data coverage	08/20–09/10	08/18–09/10	08/24–09/12
Detection limit NO_3 (ppt)			
Average	23	8	2.6
Best	2	1.5	0.8
Detection limit HONO (ppt)			
Average	320	90	38
Best	120	50	16
Detection limit NO_2 (ppb)			
Average	0.88	0.4	0.13
Best	0.24	0.2	0.05
Detection limit O_3 (ppb)			
Average	9	4	2.5
Best	4.7	1.5	0.9
Detection limit HCHO (ppt)			
Average	1	0.46	0.34
Best	0.5	0.15	0.11
Detection limit SO_2 (ppt)			
Average	260	130	180
Best	140	40	40

The last column refers to all three light paths ending at the radio tower (red, blue, and black colour in Fig. 10.3)

is due to the link of ozone photochemical formation with an increased rate of hydrocarbon oxidation, and thus HCHO production.

HCHO mixing ratios are an important parameter for the study of urban air quality. The importance of HCHO as a HO_X radical precursor is shown in Fig. 10.4. The DOAS data during PIPAPO (Fig. 10.2) were used to determine the HO_X formation due to the photolysis of O_3, HCHO, and HONO, and the ozonolysis of alkenes. In the polluted environment of Milan, HCHO photolysis is the most important HO_X precursor. The correct representation of HCHO in air quality models, as well as the accurate determination of HCHO concentrations in the field, is thus an important aspect of atmospheric chemistry research.

Finally, it should be noted here that the measurement of HCHO in the field is still a major challenge (e.g. Cardenas et al., 2000; Hak et al., 2005). The capabilities that DOAS offers for the investigation of HCHO chemistry have thus far not been entirely explored.

The photolysis of *Nitrous Acid* (HONO) can be the dominant HO_x source in the early morning, as shown in Fig. 10.4. Nitrous acid was an elusive

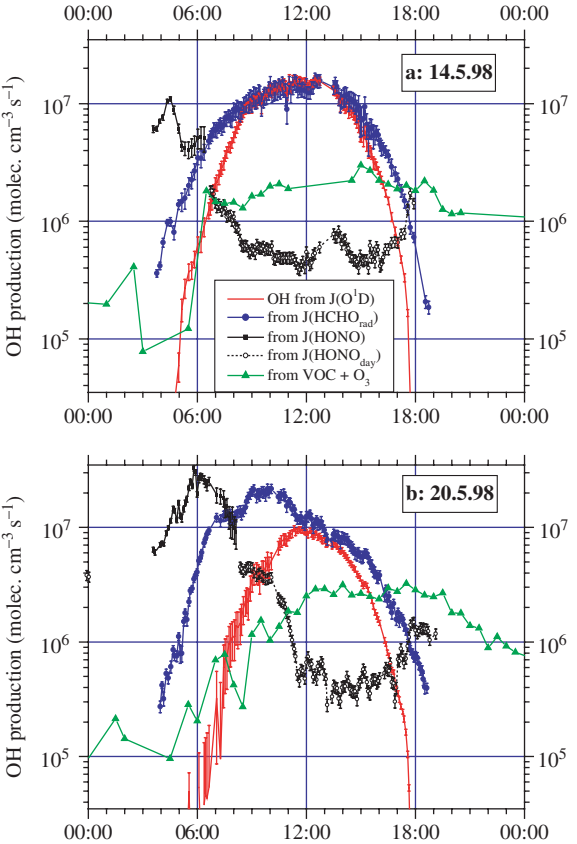

Fig. 10.4. Comparison of three different OH radical producing species for 14.5.1998 (*graph a*) and 20.5.98 (*graph b*). The data are plotted on a logarithmic scale for a better overview. The impact of HONO photolysis on the OH formation in the early morning hours can be easily seen. The estimated daytime OH production from HONO (see text) is shown with a *dotted line* (from Alicke et al., 2002, Copyright by American Geophysical Union (AGU), reproduced by permission of AGU)

compound until its discovery in the atmosphere by DOAS in 1979 (Perner and Platt, 1979). Figure 10.5 shows the first identification of HONO absorptions in a DOAS spectrum. Since the original measurement of HONO, DOAS has become the most reliable technique to measure HONO in the atmosphere. The high selectivity and the absence of interference with other trace gases, in this case primarily NO_2, make DOAS an excellent choice to measure HONO. Although the importance of HONO as a HO_X precursor has been known for decades, there are still major uncertainties about the mechanisms of its formation. It is known that HONO is formed through the heterogeneous conversion of NO_2 on various surfaces, as described in Chap. 2. Details about the nature of the surfaces or the mechanisms of the conversion are unclear. The investigation of HONO formation is thus an active field of research, where DOAS is playing an important role.

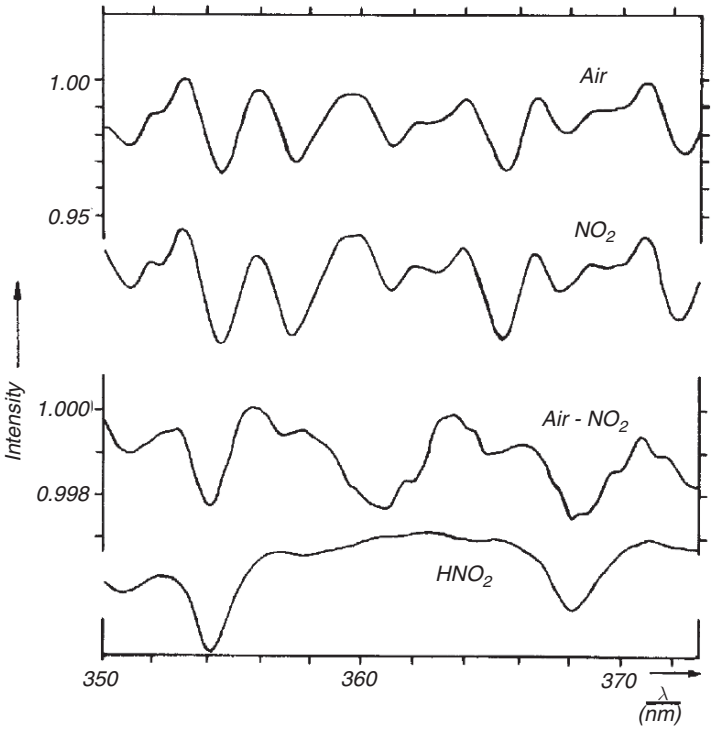

Fig. 10.5. First atmospheric absorption spectrum of nitrous acid (from Perner and Platt, 1979, Copyright by American Geophysical Union (AGU), reproduced by permission of AGU)

Modern DOAS applications have moved away from the simple measurement of HONO to more process-oriented studies of the formation of HONO. As mentioned earlier, it is suspected that the source of HONO in the atmosphere is the heterogeneous conversion of NO_2. Because DOAS measures both NO_2 and HONO in a single absorption spectrum, it offers exciting opportunities to study this chemistry.

Following the hypothesis that the formation of HONO on the ground (e.g. Perner and Platt, 1979; Stutz et al., 2004a) leads to deposition of its precursor NO_2, and release of HONO from the ground one would, therefore, expect a positive NO_2 gradient (smaller concentration at the ground than above), and a negative HONO gradient above the ground. Based on this hypothesis, Stutz et al. (2002a) set up an experiment to measure gradients and fluxes of these two species during the PIPAPO experiment. Figure 10.6 shows the set-up, which was based on a modern long-path DOAS instrument (see Chap. 7), that sequentially aimed at three retro-reflectors mounted at different heights on a 4-m-high tower. The distance between telescope and retro-reflectors was 1.25 km.

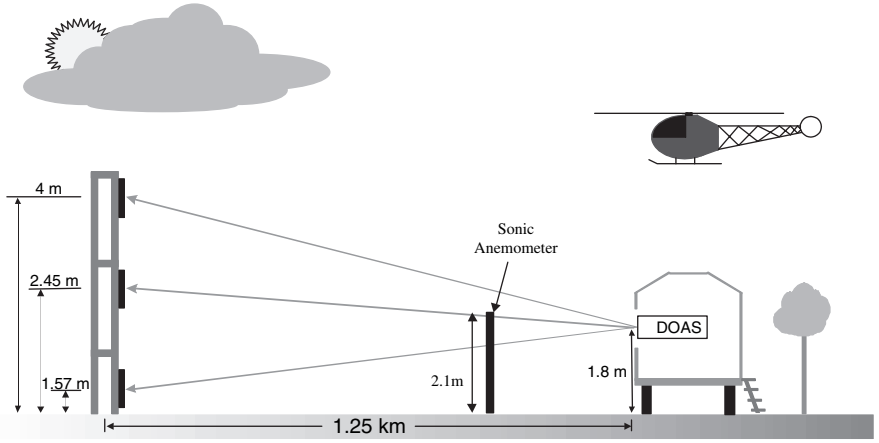

Fig. 10.6. Set-up of the experiment to measure gradients and fluxes of NO_2 and HONO during the PIPAPO experiment. The DOAS instrument aimed sequentially at the three retro-reflectors mounted on the tower at 1.25 km distance (from Stutz et al., 2002a, Copyright by American Geophysical Union (AGU), reproduced by permission of AGU)

The top panels of Figs. 10.7 and 10.8 show the NO_2 and HONO data acquired during one night. Figure 10.7, Panel b and Fig. 10.8, Panel b show the gradients calculated based on the original absorptions, where the uncertainty is determined from the error propagation of the original observations. The bottom panels then describe the fluxes and the deposition velocities of the two trace gases. The data show that during this night a deposition of both gases was observed. Based on this observation, Stutz et al. (2002a) suggest that the loss of HONO on surfaces is an important process in the atmosphere. They conclude, based on data from other nights, that the HONO loss outweighs its formation if the $HONO/NO_2$ concentration ratio exceeds $\sim 3\%$. This result shows that there is a maximum amount of HONO formation in the atmosphere. However, there are also clear indications for HONO emission from cars, in particular from DOAS studies of HONO and $HONO/NO_X$ ratios in automobile exhaust (Perner and Platt, 1980; Kessler, 1984; Kirchstetter et al., 1996; Lammel and Cape, 1996).

The example shown here illustrates how modern DOAS instruments can be used in dedicated set-ups to answer specific questions on atmospheric chemistry.

Aromatic hydrocarbon measurements are another example of successful DOAS applications. Aromatics have strong absorption features in the wavelength range 250–300 nm (Fig. 10.9). While, in principle, it should be easy to measure these absorptions in the atmosphere, several problems have to be overcome to provide accurate measurements of these species. First, the short wavelengths increase Rayleigh and Mie extinction (see Chap. 3), decreasing the maximum path length that can be achieved. In addition, strong temperature-dependent ozone absorptions are also located in this wavelength

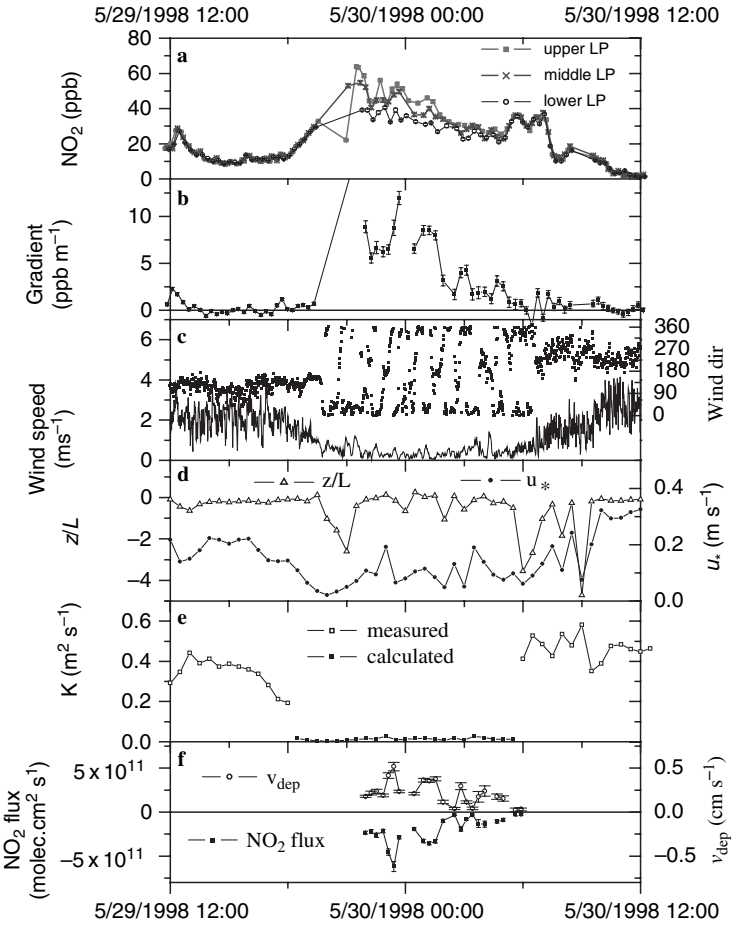

Fig. 10.7. NO_2 gradients during the night of May 29, 1998 in Milan, Italy. Gradients well above the detection limit were observed continuously for many hours during this night (from Stutz et al., 2002a, Copyright by American Geophysical Union (AGU), reproduced by permission of AGU)

window. During polluted daytime conditions, the absolute absorptions can severely reduce the transmitivity of the atmosphere. The temperature dependence of the differential absorption cross-sections is often challenging to incorporate in a DOAS analysis. Furthermore, molecular oxygen and O_2–O_2, as well as O_2–N_2 dimers, also have strong structured absorptions between 250 and 280 nm. The O_2 absorptions are in saturation at long light paths. At the limited resolution of most DOAS instruments, the shape of these absorptions thus depends mainly on the path-length in the atmosphere. Details of this effect are discussed in Chap. 6 (Sect. 6.6). Because the modelling of these absorptions based on literature cross-section is difficult, other solutions have to be found. Finally, spectrometer stray light poses a challenge for measurement

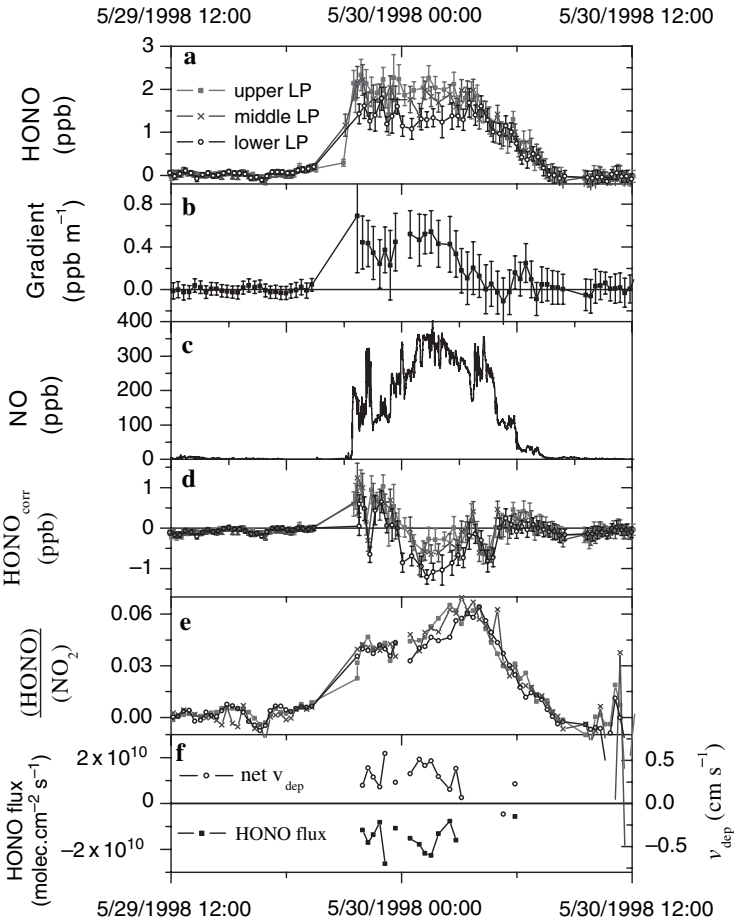

Fig. 10.8. HONO gradients during the night of May 29: (**a**) shows the mixing ratios on the individual light paths (LP). The gradient is displayed in (**b**). To remove the influence of direct HONO emissions, we calculated $HONO_{corr}$ by subtracting 0.65% of the NO_x (not shown here) from the HONO mixing ratios (**d**). The ratio of HONO to NO_2 mixing ratios is displayed in (**e**). The fluxes and net deposition velocities is shown in (**f**) (from Stutz et al., 2002a, Copyright by American Geophysical Union (AGU), reproduced by permission of AGU)

in the UV. Many light sources used in active DOAS have their emission maximum in the visible range and thus provide low intensity in the UV. The imperfect suppression of visible light in spectrometers leads to stray light levels that can be 10% and more of the signal between 250 and 300 nm.

Long-path DOAS measurements in the atmosphere, both for research and for air quality monitoring purposes with commercial instruments, have been reported during a number of occasions. Frequently, the problems with the O_2 and O_2–O_2/O_2–N_2 dimer absorptions are solved by ratioing the measured spectrum to a spectrum recorded on the same light path. The difficulty with

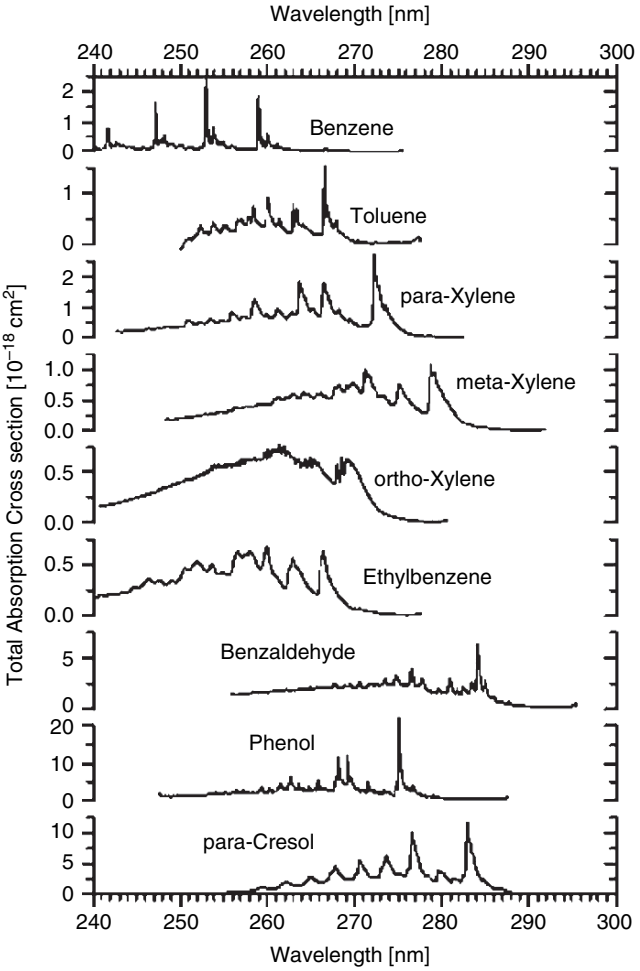

Fig. 10.9. Absorption cross-section of various aromatic hydrocarbons in the UV wavelength range

this approach is to determine the atmospheric concentration of aromatics at the time this reference spectrum is recorded. If the level of aromatics is not known, only relative measurements can be performed. The temperature-dependent ozone absorption can, for example, be modelled by including ozone reference spectra for different temperatures in the fit. Spectrometer stray light is reduced by either using UV band-pass filters or by correcting the stray light

The determination of aromatics in the atmosphere is a promising application of DOAS, in fact a series of measurements have been reported (e.g. Löfgren, 1992; Senzig, 1995; Axelsson et al., 1995; Barrefors, 1996; Volkamer et al., 1998; Volkamer, 2001; Kurtenbach et al., 2001). However, we will discuss here another application: the measurement of aromatic hydrocarbons in

a traffic tunnel to determine the emission ratios of these species from an average car fleet. The measurements were made by Kurtenbach et al. (2001) with a open-path multi-reflection DOAS instrument with a base-path length of 15 m inside a tunnel in Wuppertal, Germany. The cell was operated on a total path-length of 720 m. Details of the White cell set-up can be found in Chap. 7. The time resolution of the measurements was ~ 1 min, much faster than typical gas chromatographs (GCs).

The multi-reflection cell offers a number of advantages with respect to the measurement of aromatics. The most important advantage is the ability to enclose the optics and flush it with clean air to derive a reference spectrum of O_2 and O_2–O_2/O_2–N_2 dimer absorptions. If this is not feasible, one can derive such a spectrum from open-path measurements with a collocated GC. The determination of the aromatics from the GC is more representative for a multi-reflection cell that only probes a small volume. For the multi-reflection cell measurements by Kurtenbach et al. (2001) and Ackermann (2000), both approaches were used.

To ensure that small temporal changes in the instrument function do not influence the analysis of the spectra, in particular for the strong O_2 absorptions, a cross-convolution technique is applied. In this method, the atmospheric spectrum is convoluted with the instrument function of the O_2 reference spectrum (and if measured at the same time also of the reference spectra of the aromatics), while the reference spectra are convoluted with the instrument function of the atmospheric spectra (Volkamer et al., 1998). After this procedure, both sets of spectra have the same characteristics and can be analysed with the DOAS method.

To overcome challenges with spectrometer stray light, two measurements were performed. The first measurement was performed without any additional filters in the light beam. During the second measurement, a long-pass filter (Schott WG305) blocked light of wavelengths below 300 nm. This spectrum thus determines the spectrometer stray light originating from wavelengths above 300 nm. Because the maximum intensity of the Xe-arc lamp employed during the measurements is around 500 nm, this is the major portion of the spectrometer stray light. The measurement with the filter was then subtracted from the first measurement to derive the true spectrum between 250 and 300 nm. This spectrum was analysed using the methods of Chap. 8 and the cross-convoluted spectra. All aromatic reference spectra in the study of Kurtenbach et al. (2001) were measured with the instrument in the field and then later calibrated with the absorption cross-sections by Etzkorn et al. (2000), because no high resolution absorption cross-sections for aromatics are currently available. The O_2 reference spectrum was measured at exactly the same path length that was later used in the tunnel measurements by filling a Teflon tube around the multi-reflection cell with synthetic air. The top panel of Fig. 10.10 shows an example of a tunnel measurement of various aromatic hydrocarbons. The absorptions are clearly identified.

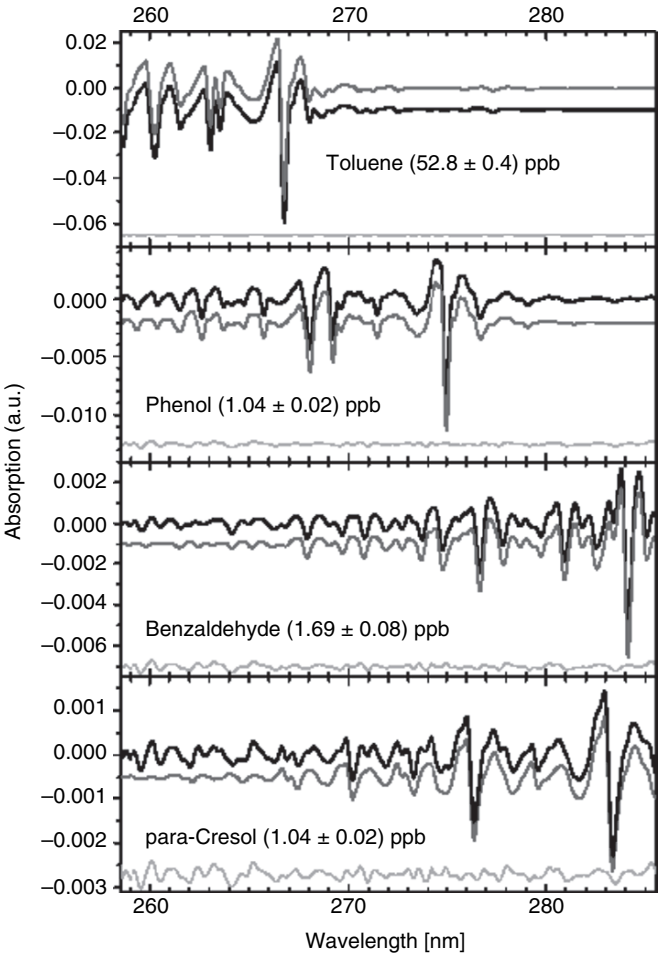

Fig. 10.10. Example of an analysis of toluene, phenol, benzaldehyde, and p-cresol measured in a traffic tunnel. The figure compares the scaled reference spectrum with the sum of this spectrum and the residual. This comparison gives a visualisation of the quality of the fit. Also shown are the residual specta (thin lines near the bottom of each panel), which in this case were much smaller than the absorptions of the trace gases (from Ackermann, 2000)

Table 10.3 lists the maximum mixing ratio observed from the various aromatics in the tunnel, as well as the detection limits of the measurements. For benzene and toluene, the detection limit is on the order of 1 ppb. For other aromatics, such as benzaldehyde and p-cresol, the detection limits are even lower. While the detection limits are greater than those from GC measurements, the DOAS system is much faster (1 min compared with 20 min) and needs no calibration.

Table 10.3. Detection limit of various aromatic hydrocarbons during the tunnel measurements in Wuppertal (from Ackermann, 2000)

Species	Highest mixing ratio observed (ppb)	Detection limit (ppb)
Benzene	36.8	0.6
Toluene	83.9	0.7
Ethyl-benzene	18.1	0.8
Benzaldehyde	2.2	0.07
para-Xylene	13.0	0.3
meta-Xylene	11.0	1.0
ortho-Xylene	20.0	2.0
Phenol	2.80	0.15
para-Cresol	1.07	0.03
SO_2	33.0	0.5

The time traces of 1 week of measurements (Fig. 10.11) show that the levels of aromatics in the tunnel depend strongly on the traffic density (top trace in Fig. 10.11), as one would expect from pollutants that originate from vehicular emissions.

Ackermann (2000) used the data from the tunnel measurements to derive the emission factors for the various aromatic hydrocarbons (Table 10.4). These parameters are essential for the conditions in urban air quality models that are used to develop mitigation strategies for urban pollution. This example shows that DOAS can contribute in other ways to solve today's air pollution problems than the simple monitoring of trace gas concentrations.

Ammonia plays an important role as a reducing agent in the atmosphere. Through reaction with acids, such as H_2SO_4 and HNO_3, it contributes to the formation of particular matter, and is thus an important component of smog. High numbers of particles are often found in areas where urban pollution is mixed with rural air containing elevated levels of NH_3. The most important sources of ammonia are the bacterial activity in the decomposition of animal waste, in the soil, and biomass burning.

Measurements of ammonia with DOAS have, for example, been reported for flue gas analysis (Mellqvist and Rosén 1996) as well as in ambient air (Neftel et al., 1990). Here, we show an example for the measurement of ammonia concentrations at a dairy farm. Mount et al. (2002) used a coaxial long-path DOAS system with an array of retro-reflectors located at a distance of up to 150 m (Fig. 10.12). The main difference to the set-ups described in Chap. 7 is the introduction of a double spectrograph, for improved stray light suppression in the UV. Because NH_3 absorbs between 190 and 220 nm (Fig. 10.13, right panel), at even smaller wavelengths than aromatics, stray light suppression is critical for this application, as explained.

The left panel of Fig. 10.13 shows an example of a raw spectrum recorded with the instrument shown in Fig. 10.12. The intensity rapidly decreases

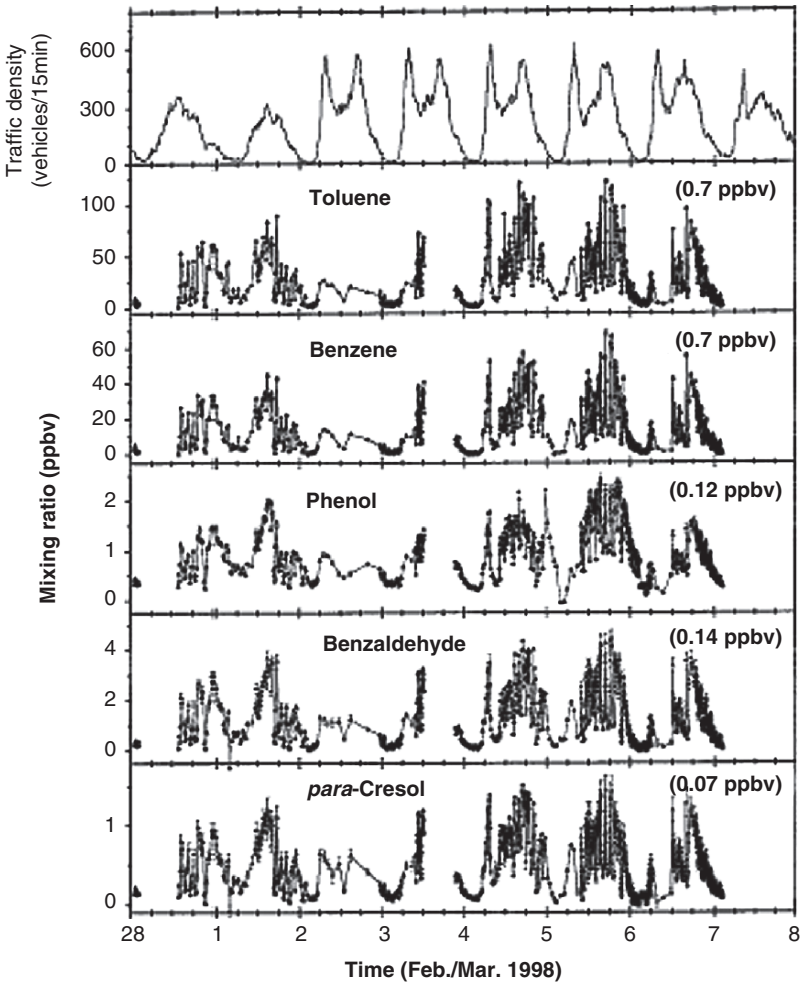

Fig. 10.11. Diurnal variations of the mixing ratios of various aromatic hydrocarbons during the first week of February 1998. Measurements were made with an open multi-reflection system inside a traffic tunnel in Wuppertal, Germany (Ackermann, 2000; Kurtenbach et al., 2001). The *top panel* shows the traffic density in the tunnel. The *numbers* in parenthesis denote the detection limits of the respective aromatics (from Kurtenbach et al., 2001)

towards shorter wavelengths. In general, the light intensity is low compared with long-path instruments operating in the visible range. However, the intensity is sufficient to allow the identification of ammonia in ambient air. The right panel of Fig. 10.13 shows a comparison of a spectrum measured with the light path passing over a NH_3 source compared with a differential absorption cross-section of NH_3. Taking into account saturation effects in the raw ratio, the agreement between the two curves is excellent.

Table 10.4. Emission factors for aromatic hydrocarbons derived from DOAS measurements in a traffic tunnel (from Ackermann, 2000)

Species	Emission factors (milligram per vehicle kilometre driven)		
	Weekday	Weekend	Total
Toluene	56.7 ± 4.5	60.5 ± 8.5	58.0 ± 5.0
Benzene	24.7 ± 1.9	27.8 ± 7.2	25.4 ± 3.2
Ethyl-benzene	18.5 ± 1.5	24.3 ± 4.1	19.2 ± 2.3
Benzaldehyde	1.62 ± 0.12	3.4 ± 0.5	1.1 ± 0.2
Para-xylene	7.4 ± 0.6	9.1 ± 1.4	7.3 ± 0.8
Meta-xylene	8.9 ± 0.8	10.4 ± 1.6	9.2 ± 1.1
Ortho-xylene	17.7 ± 1.5	25.8 ± 5.6	18.4 ± 2.1
Phenol	1.44 ± 0.12	1.76 ± 0.35	1.5 ± 0.2
P-cresol	0.85 ± 0.10	1.25 ± 0.21	0.89 ± 0.10

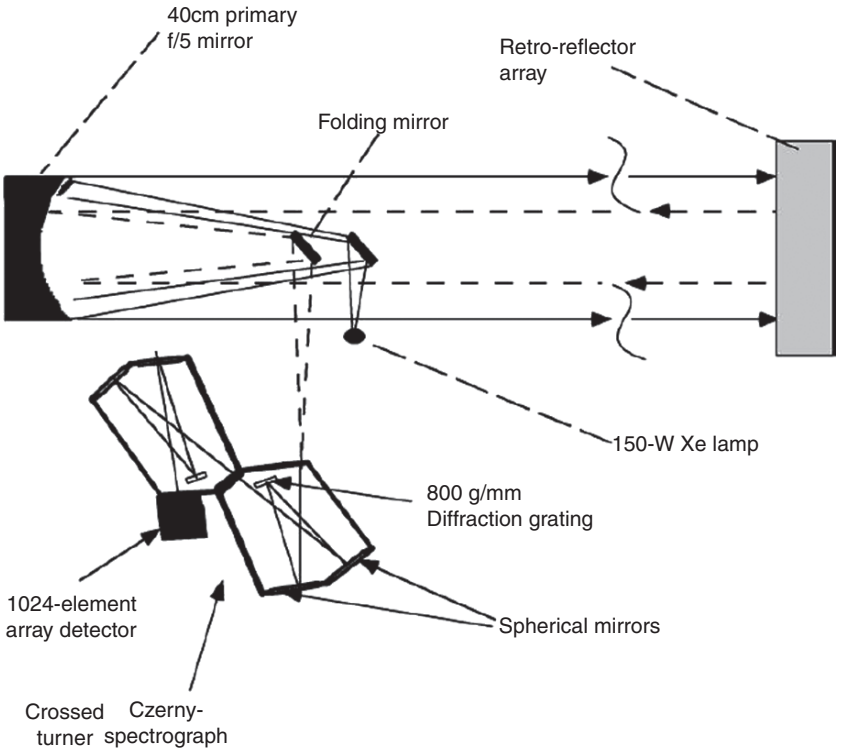

Fig. 10.12. Instrumental set-up for the measurement of ammonia emission from a dairy farm (from Mount et al., 2002, Copyright Elsevier, 2002)

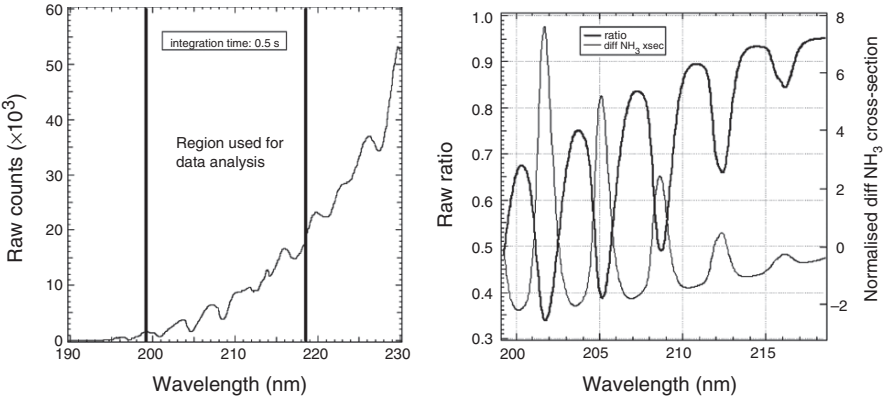

Fig. 10.13. Left panel: Raw spectrum measured on a 68 m path with an integration time of 0.5 s (Mount et al., 2002).The decrease of the intensity towards shorter wavelengths can be clearly seen. **Right panel**: Comparison of the ratio of two spectra with and without NH_3 in the light beam, to the absorption cross-section of NH_3. The difference in shape is caused by saturation effects in the raw ratio (from Mount et al., 2002, Copyright Elsevier, 2002)

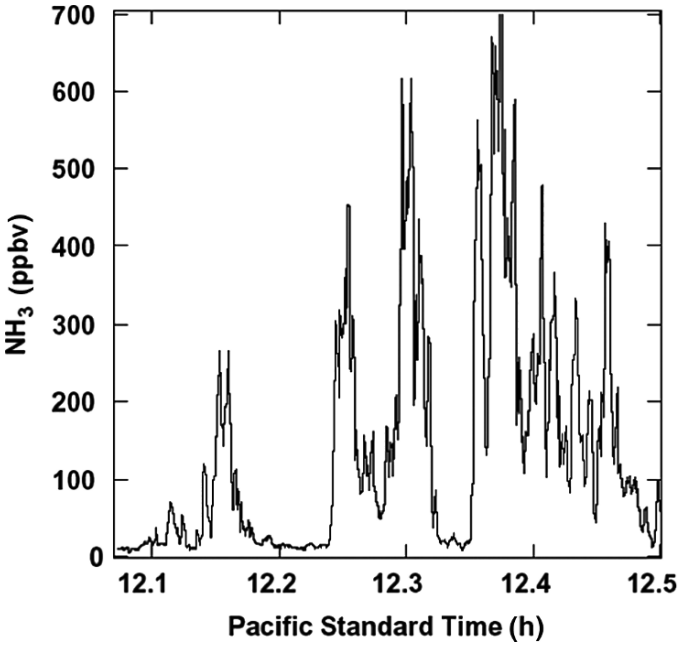

Fig. 10.14. Example of ammonia mixing ratios measured downwind of a slurry lagoon (Mount et al., 2002). The integration time for one measurement was 0.6 s (from Mount et al., 2002, Copyright Elsevier, 2002)

Mount et al. (2002) used this instrument to monitor the release of ammonia on a diary farm. Figure 10.14 shows 1 h of high frequency measurement downwind of a slurry lagoon. The rapid variations are caused by shifting winds and turbulent cells moving into the light path.

The observations by Mount et al. (2002) illustrate how active DOAS instruments can be applied to fence-line monitoring, in this case of the release of ammonia from a dairy farm. The potential of DOAS for the measurement of NH_3 has thus far not been extensively explored and there is great potential for further developments.

10.1.2 Vertical Profiles of Air Pollution by Multiple DOAS Light Beams

As we already described above, active DOAS instruments can be used to measure the vertical distribution of trace gases. This was first explored by Platt in 1977, with the goal of measuring SO_2 deposition velocities. While this technique was not used for nearly two decades, it was revived recently to study nocturnal chemical processes. The investigation of NO_2 to HONO conversion was a first example of vertical profiling. Here, we want to discuss another example that was set up to study the vertical variation of nocturnal chemistry.

Two long-path DOAS instruments were set up in Houston, Texas, during TEXAQS 2000 (see also Sect. 10.1.1 above). The measurements were made on five different light paths, as illustrated in Fig. 10.15. The first DOAS system measured on the two short light paths taking $\sim$ 5 min for one series of measurements. The second system took $\sim$ 15 min to measure all three long light paths. The raw data of these measurements are shown in Fig. 10.3.

A simple deconvolution process was then used to derive trace gas mixing ratios averaged in the boxes indicated in Fig. 10.15. Because the measurements were made sequentially, all data were linearly interpolated to the time of the upper long path measurement. The path integrated concentration along the ith light path is denoted as S_i, and the concentrations in a specific height interval as C_i, where the light paths are numbered from the ground upwards.

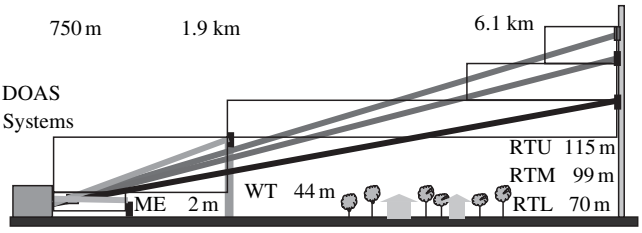

Fig. 10.15. Set-up during the TEXAQS 2000 experiment. Five retro-reflector arrays were mounted at different distances and altitudes. The measurements were performed by two DOAS instruments (from Stutz et al., 2004b, Copyright by American Geophysical Union (AGU), reproduced by permission of AGU)

The data of the two lowest paths directly represent the concentrations at 2-m altitude and in the height interval (2–44 m). The other concentrations C_3, C_4, and C_5 in the height intervals, respectively, (44–70 m), (70–99 m), and (99–115 m) are calculated from the ground upwards with the following equation:

$$C_i = \frac{h_i - H}{h_i - h_{i-1}} S_i - \frac{h_{i-1} - H}{h_i - h_{i-1}} S_{i-1}.$$

An important assumption, which underlies the application of this equation, is that the trace gases are homogeneously distributed in the horizontal direction. This can be tested by using a number of techniques outlined by Stutz et al., 2004b. It is also essential to determine the errors of the concentrations averaged over the height intervals. Since differences of the measurements are formed and the effective absorptions path in the boxes is shorter than the initial path length, the errors of the box averaged concentrations increase. One has to be careful to assess whether the measured concentrations are statistically meaningful. Four days of box-averaged mixing ratios during times when horizontal uniformity was encountered and statistically significant trace gas levels were found are shown in Fig. 10.16. During a number of instances vertical profiles of the various trace gases were observed. Clearest are the

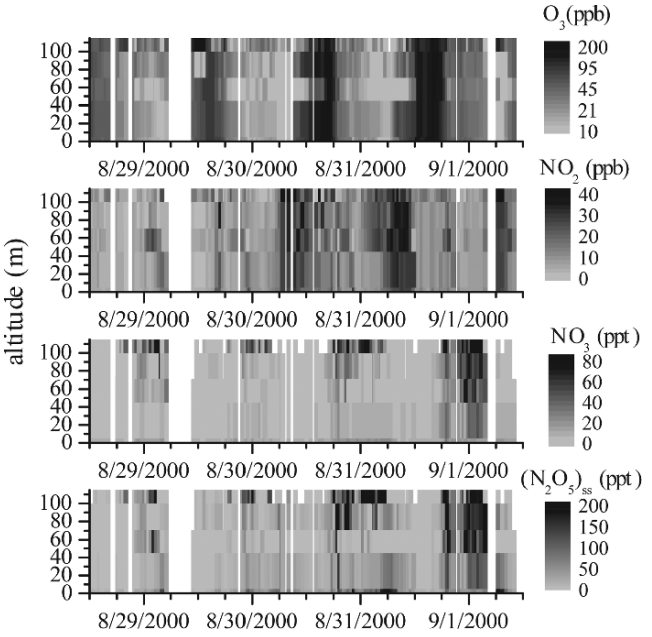

Fig. 10.16. Observations of the spatial distribution of trace gas mixing ratios during 4 days in Houston, TX. The N_2O_5 mixing ratios are calculated from the steady state of measured NO_2, NO_3, and N_2O_5. The O_3 mixing ratios are displayed in a logarithmic colour coding (from Stutz et al., 2004b, Copyright by American Geophysical Union (AGU), reproduced by permission of AGU)

nocturnal maxima of NO_3 in the upper nocturnal boundary layer each night. On several occasions, vertically non-uniform distributions of O_3 and NO_2 are observed. For example, on August 31, a plume of NO_2 between 50 and 90 m was encountered.

The nocturnal profiles of the various gases are more clearly seen in Fig. 10.17. The profiles show that the levels of all gases vary with altitude. This variation, and in particular that of NO_3, the dominant nocturnal radical, leads to an altitude-dependent nocturnal chemistry. Similar experiments

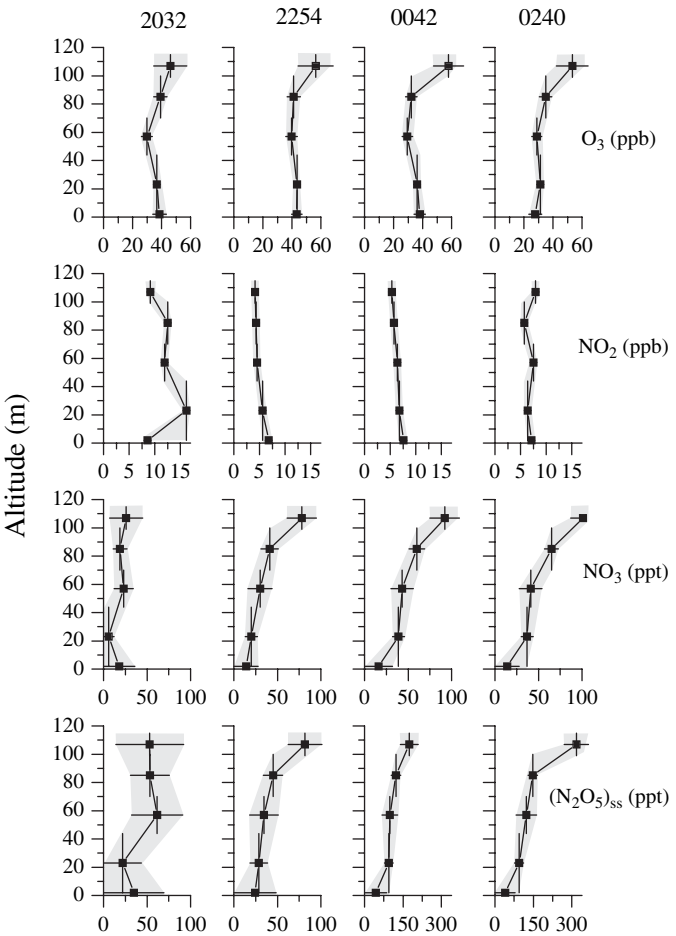

Fig. 10.17. Vertical mixing ratio profiles of O_3, NO_2, NO_3, and N_2O_5 near Houston, Texas (USA) during the night of 8/31-9/1, 2000 at four different times (noted on *top of the graphs*). The N_2O_5 mixing ratios shown are calculated from the steady state of measured NO_2, NO_3, and N_2O_5 (from Stutz et al., 2004b, Copyright by American Geophysical Union (AGU), reproduced by permission of AGU)

have confirmed these results. Figures 10.16 and 10.17 show examples of the abilities of modern DOAS instruments to perform process studies in the atmosphere. Active DOAS continues to contribute to the advancement of our understanding of pollution in the atmosphere.

10.2 Investigation of Free Radical Processes in the Atmosphere

As outlined in Chap. 2, free radicals play a central role in many chemical systems, such as flames, living cells, or in the atmosphere. Due to their high chemical reactivity, radicals are the driving force for most chemical processes in the atmosphere. In particular, they initiate and carry reaction chains. Thus, knowledge of the concentration of those species in the atmosphere is a key requirement for the investigation of atmospheric chemistry. For instance, degradation of most oxidisable trace gases in the atmosphere, such as hydrocarbons, carbon monoxide, or H-CFC's, is initiated by free radicals.

As a consequence of their high reactivity, the steady state concentration of free radicals in the atmosphere is generally quite low, even compared with atmospheric trace gas standards. For instance, the atmospheric lifetime of the OH radical never exceeds 1 s. A consequence of this short lifetime is that transport processes can be largely neglected when considering the budgets of most free radicals. Therefore, measurement of the instantaneous concentration of free radicals together with a comprehensive set of other trace gases linked with the radical's chemical cycles allows the study of in situ chemical reactions in the atmosphere (Perner et al., 1976, 1987a; Platt et al., 1987, 1988, 2002;

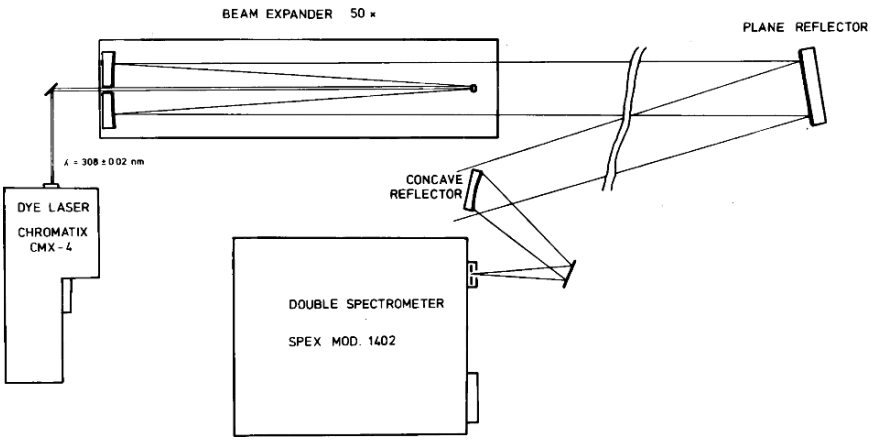

Fig. 10.18. Optical set-up of the high-resolution DOAS instrument used for the first reliable detection of OH in the atmosphere (Perner et al., 1976). A broadband, frequency-doubled dye laser serves as light source

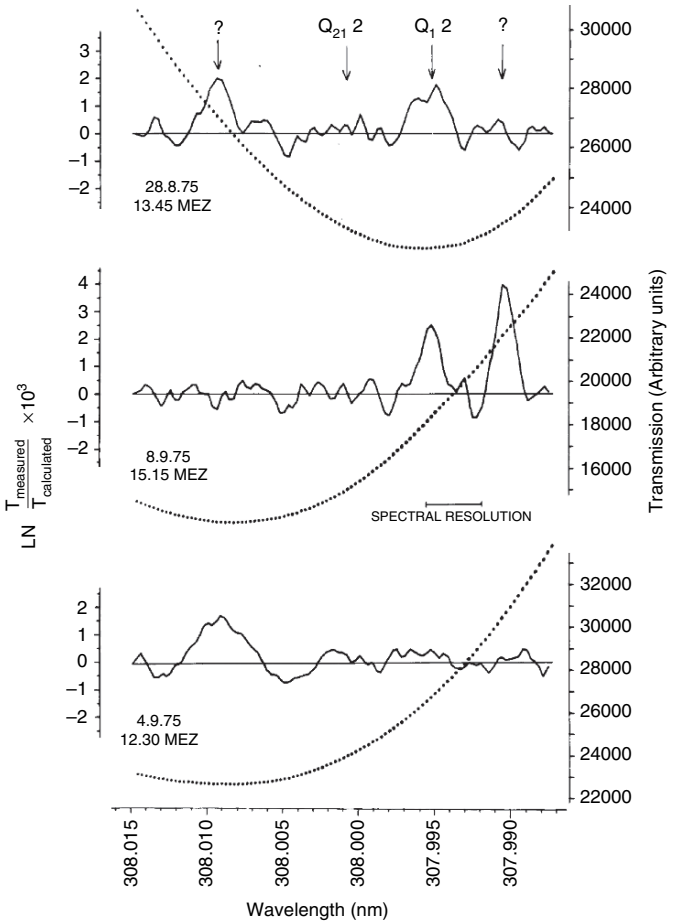

Fig. 10.19. High-resolution spectrum of OH. The DOAS instrument was used for the first reliable detection of OH in the atmosphere (from Perner et al., 1976, Copyright by American Geophysical Union (AGU), reproduced by permission of AGU)

Dorn et al., 1988, 1993, 1996; Mount 1992; Mount and Eisele, 1992; Eisele et al., 1994; Brauers et al. 1996, 1999; Hausmann et al., 1997; Hofzumahaus et al., 1998).

Several key free radicals of interest to atmospheric chemistry can be measured by DOAS with very high (sub – ppt) sensitivity. To date, the following radicals have been measured: Hydroxyl radicals (OH), nitrate radicals (NO_3), and halogen oxide radicals (ClO, OClO, BrO, OBrO, IO, and OIO). In fact, most of them were detected for the first time in the atmosphere by DOAS.

In this section, we will discuss some examples of the measurement of these radical species. Again, we can only show examples of the many measurements that have been made of radical species.

10.2.1 Measurement of OH Radicals by DOAS

A series of OH measurement campaigns were performed with the DOAS technique, initially using optomechanical scanning of the spectra (Perner et al., 1976, 1987a, Platt et al., 1988), and in later instruments employing diode array detectors (Dorn et al., 1988; Hofzumahaus et al., 1991), see Sect. 7.9.2. Observed OH radicals levels ranged from the detection limit ($1–2 \times 10^6$ molec. cm^{-3}) to about 10^7 molec. cm^{-3}. Figures 10.18, 10.19, and 10.20 show the optical set-up using a frequency doubled dye laser as light source, examples of a spectrum and a diurnal profile of the OH concentration.

The most recent implementations of DOAS OH instruments are based on multi-reflection cells with base path lengths of 20–40 m (Brauers et al., 1996). This instrument reaches detection limits down to 1.5×10^6 molec. cm^{-3} in an integration time of about 200 s. Figure 10.21 shows the different absorption features that can be found in the wavelength window used for the measurement of OH. In particular, interferences of SO_2, HCHO, and naphthalene are observed.

Figure 10.22 shows the identification of the OH absorptions in an atmospheric spectrum. The spectrum was measured using the multi-channel scanning technique (MCST), which is explained in detail in Sect. 7.14.2. It should be noted that the amplitude of the residual is extremely low in this measurement, with a peak-to-peak equivalent optical density of $\sim 10^{-4}$.

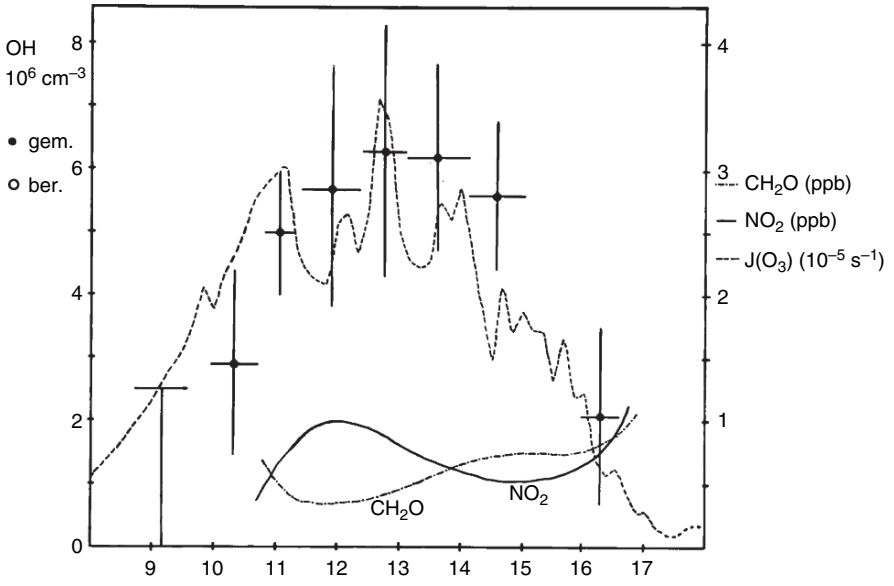

Fig. 10.20. Diurnal OH profile measured with a later version of the OH DOAS instrument (see Fig. 7.48) (from Platt et al., 1987)

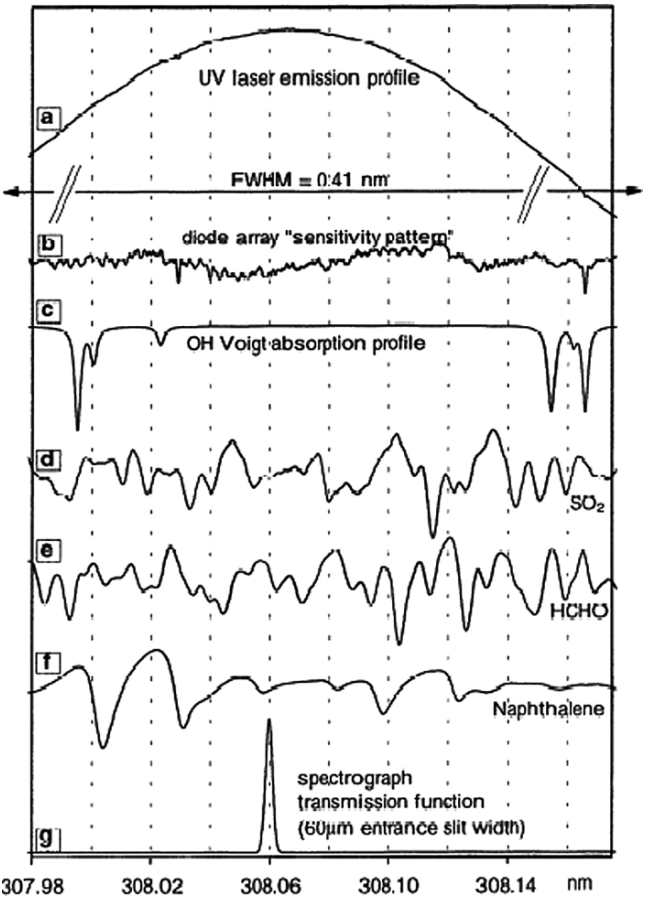

Fig. 10.21. OH absorption spectrum (*trace c*) together with the spectra of several interfering species SO_2, CH_2O, and naphthalene (*traces d–f*). Also shown are the laser intensity profile (*trace a*) and the diode array sensitivity pattern (from Brauers et al., 1996, Copyright by American Geophysical Union (AGU), reproduced by Permission of AGU)

The measurements in Figs. 10.20 and 10.23 show the diurnal profile of OH with a maximum around noon. The comparison of the OH concentration with $J(O^1D)$ in Fig. 10.23, confirms the strong influence of solar radiation on OH levels.

10.2.2 Measurement of NO_3 Radicals

Nitrate radicals, NO_3 and OH, are in a sense complementary to each other (see Chap. 2): OH radicals are directly produced by photochemical reactions, thus their concentration is highest at noon and low at night. Conversely, nitrate radicals are effectively destroyed during the day, thus they will reach high

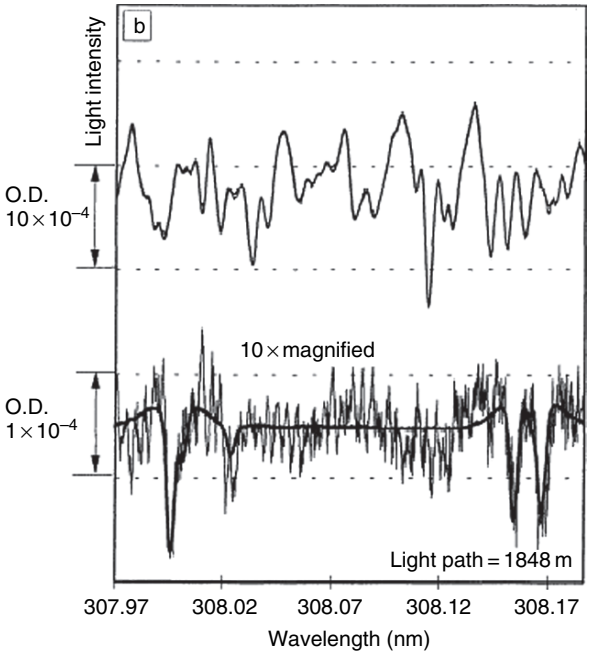

Fig. 10.22. Ambient OH measurement in Pennewitt, Germany, August 16, 1994. The atmospheric spectrum (*top trace*) is dominated by the absorptions of SO_2 as shown in *trace d* of Fig. 10.21. After the removal of this absorption, the structures of OH can be clearly identified in the spectrum (*bottom trace*). The absorptions correspond to an OH concentration of $8.8 \cdot \times 10^6$ molec. cm^{-3} (from Brauers et al., 1996, Copyright by American Geophysical Union (AGU), reproduced by permission of AGU)

concentrations predominately at night. Both species are responsible for the removal of hydrocarbons and NO_X from the atmosphere. The product of NO_3 and OH reactions with NO_2 is nitric acid. We already discussed the role DOAS played in the detection of OH radicals. Here, we will concentrate on the importance of DOAS measurements for nocturnal radical chemistry, i.e. NO_3 chemistry.

NO_3 was first identified in the troposphere spectroscopically by Platt et al. (1979) and Noxon et al. (1980). Figure 10.24 shows the first reported NO_3 measurement by active DOAS. Due to the width of the NO_3 absorption bands and location in the visible part of the spectrum NO_3 can readily be measured by active DOAS using a variety of thermal light sources (incandescent lamps, Xe-arc lamps). Since then a large number of NO_3 measurements in the atmosphere have been reported (Platt et al., 1980a, 1981, 1984, 1990; Harris et al., 1983; Brauers et al., 1990; Platt, 1991; Plane and Nien, 1991; Winer and Biermann, 1991; Platt and Heintz, 1994; Platt and Hausmann, 1994; Plane and Smith, 1995; Platt and Janssen, 1996; Heintz et al., 1996; Carslaw et al., 1997; Aliwell

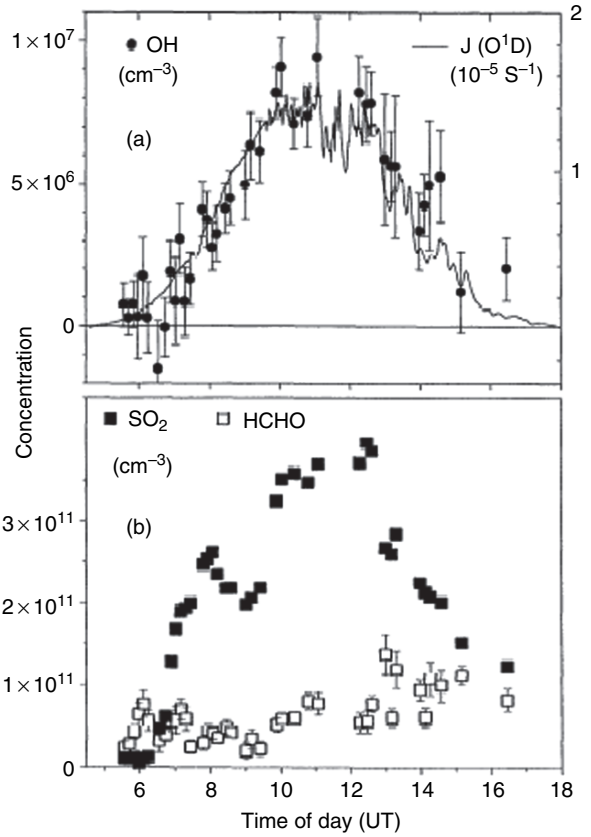

Fig. 10.23. Diurnal profiles of OH concentration and ozone photolysis frequency at a rural site in north-eastern Germany (**top panel**). Also shown are the concentrations of HCHO and SO_2 that are determined in the measurement (**bottom panel**) (from Dorn et al., 1996, Copyright by American Geophysical Union (AGU), reproduced by permission of AGU)

and Jones, 1998; Allan et al., 1999, 2000; Geyer et al., 1999, 2001a,b,c; Gölz et al., 2001; Ball et al., 2001; Geyer and Platt, 2002; Stutz et al., 2002; Kurtenbach et al., 2002; Geyer et al., 2003; Kern et al., 2006). A challenge in the measurement of NO_3 is the interference with a water-absorption band system around 650 nm (see, e.g. Fig. 10.26). Because the spectral structure of this band system is much narrower than that of NO_3 filtering procedures are often used to reduce the effect of water (Geyer et al., 1999). Another method to remove this water band is the use of daytime atmospheric spectra as water references. This technique has been employed in most NO_3 measurements in the past (see top panel in Fig. 10.27). However, as pointed out recently by Geyer et al. (2003), NO_3 levels can be elevated under conditions with high O_3 mixing ratios ($[O_3] > 100$ ppb) during the day. In this case, more care has

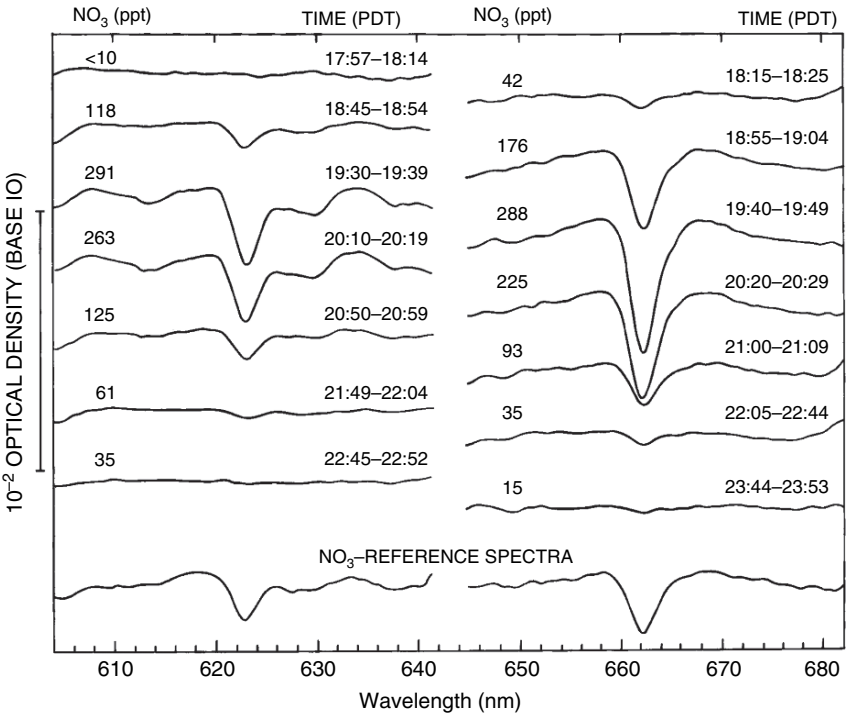

Fig. 10.24. Example of NO_3 radical spectra recorded in an urban area (Riverside, Los Angeles, USA). The absorption structures due to H_2O and O_2 are already removed (from Platt et al., 1979, Copyright by American Geophysical Union (AGU), reproduced by permission of AGU)

to be taken in the choice of water reference spectra, i.e. Geyer et al. (2003) used daytime spectra taken during periods of high NO mixing ratios as water references.

Because DOAS is the most commonly used technique to measure the atmospheric concentration of NO_3, there are many examples of its application. Figures 10.24 and 10.26 show NO_3 spectra in an urban and rural environment, respectively. Figure 10.25 presents the corresponding time series of NO_3 after sunset in an urban environment. Because NO_3 also plays an important role in marine areas, we also show an example taken in the remote marine boundary layer (Fig. 10.27). This spectrum illustrates that very low NO_3 mixing ratios, close to 1 ppt, can be measured accurately.

Observations in the Marine Boundary Layer

A number of NO_3 DOAS observations in the marine boundary layer have been reported (e.g. Heintz et al., 1996; Martinez et al., 2002). Here, we will review data measured at Mace Head, Ireland and Weybourne, England (Allan et al., 2000; Carslaw, 1997).

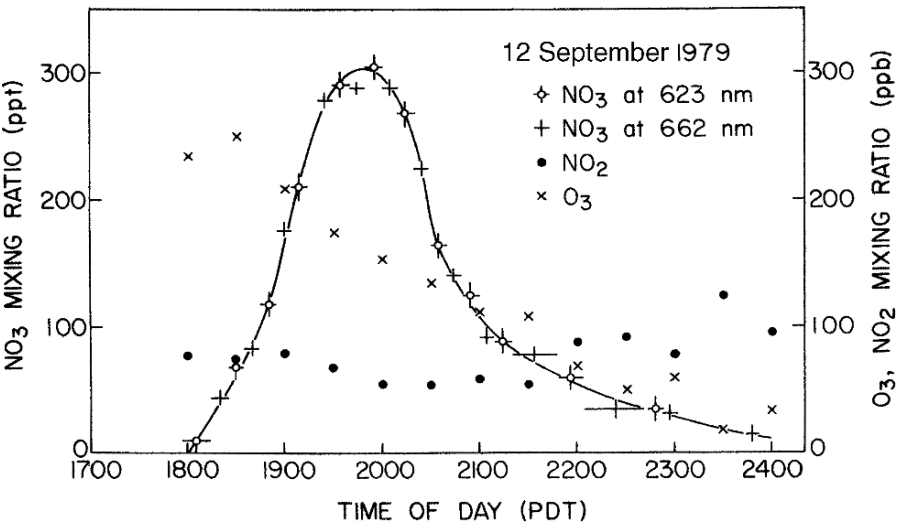

Fig. 10.25. Example of NO_3 radical time series in an urban area (Riverside, Los Angeles, USA) after sunset. Data are derived from the series of spectra shown in Fig. 10.24. (from Platt et al., 1979, Copyright by American Geophysical Union (AGU), reproduced by permission of AGU)

Figure 10.28 shows an overview of a time series of NO_3 measurements. The maximum NO_3 mixing ratios observed at Mace Head are up to 40 ppt. A clear dependence on the origin of the air is observed. Clean atlantic or polar air has low NO_3 levels, while continental air shows much higher NO_3. This can be explained by the much higher NO_x levels in these air masses, which increases the formation rate of NO_3.

The data in Fig. 10.28 can be used to derive the removal rate of NO_X at night through the calculation of N_2O_5 and its uptake on the aerosol. In addition, it can be used to determine the nocturnal oxidation of DMS. Figure 10.29 shows another application of these measurements by showing a comparison of NO_3 and $HO_2 + RO_2$ levels. This correlation is due to the oxidation of organic species by NO_3 at night (see Sect. 2.5.2).

Observations in Rural and Forested Areas

Measurements of NO_3 in rural and forested areas are of particular significance since emissions of mono-terpenes, which rapidly react with NO_3, are often highest there. A continental long-term study was reported at the continental site Lindenberg near Berlin, Germany by Geyer et al. (2001) (Fig. 10.30). Observations of this type offer the possibility of statistical investigations of the night-time NO_3 and N_2O_5 concentrations and the NO_3 production and

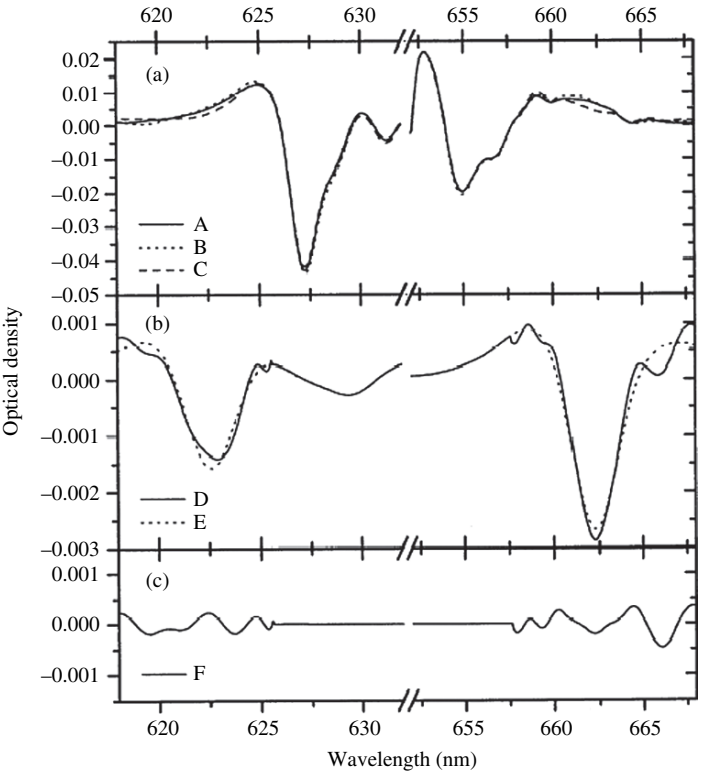

Fig. 10.26. Example of night-time NO_3 radical absorption in a rural area (August 5, Pabsthum, Germany). (Geyer et al., 1999). The *top panel (a)* shows the atmospheric spectrum at 2150 UT **(trace A)** and two daytime references (**traces B, C**), which are dominated by water absorptions. The *middle panel (b)* shows a comparison of the scaled NO_3 reference with added residual (**D**) and the NO_3 reference (E)). The optical density of NO_3 absorption is $\sim$ 0.35% which, in this case, was equivalent to 9.8 ± 1.1 ppt. The *bottom panel (c)* shows the residual of the analysis (**trace F**). Details about the analysis procedure can be found in (from Geyer et al., 1999, Copyright by American Geophysical Union (AGU), reproduced by permission of AGU)

degradation frequencies, see Sect. 2.5. In addition, the mean contribution and the seasonal variation of the different sink mechanisms of NO_3, which provides an essential tool for quantifying the average effect of NO_3 on the oxidation capacity of the atmosphere, can be studied.

Observations in Urban Areas

Figure 10.24 showed examples of urban spectra of NO_3. Surprisingly, few measurements of NO_3 have been performed in this environment. This is partially

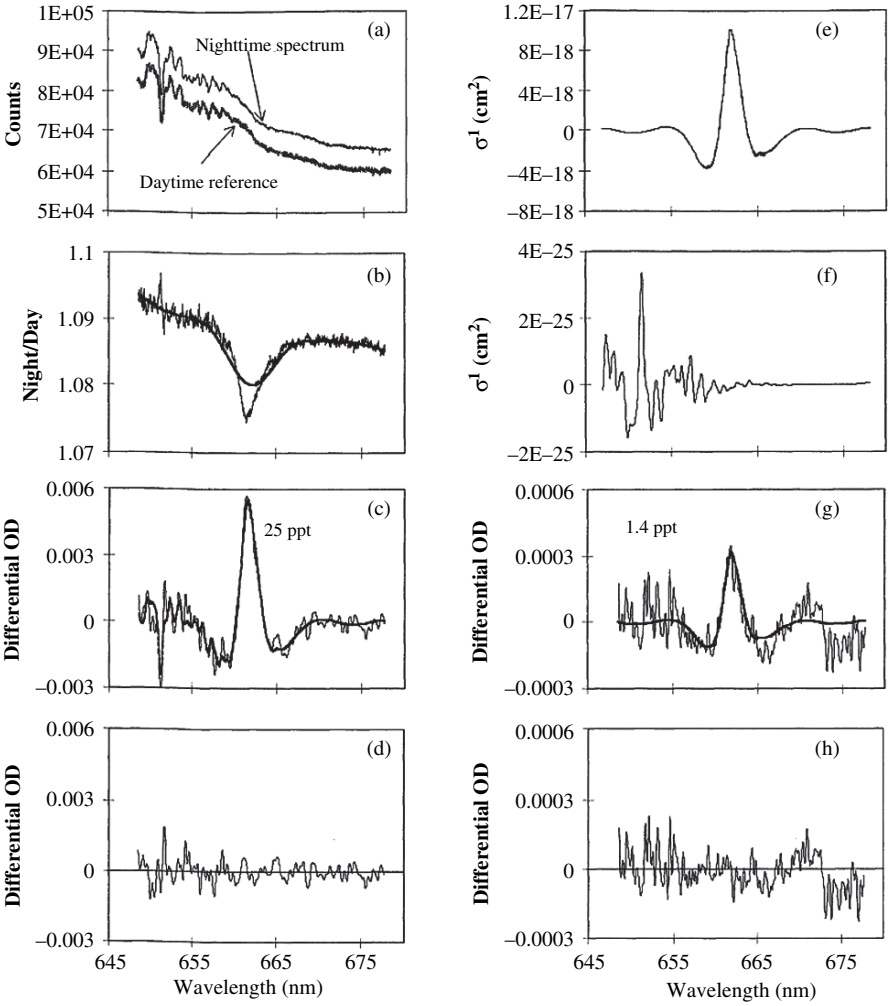

Fig. 10.27. Example of night-time NO_3 radical absorption in the marine boundary layer (Allan et al., 2000): (**a**) shows the daytime reference and the nocturnal spectrum; (**b**) is the ratio of the two spectra with a low-pass filter; (**c**) and (**g**) show the fit of the H_2O and NO_2, cross-sections (**e and f**) and (**d**) is the residual. The result of the fit gave a NO_3-mixing ratio of 24.7 ± 0.7 ppt. An example with 1.9 ± 0.2 ppt of NO_3 is shown in (**g**). The measurements were made with a long-path DOAS instrument on a 8.4-km-long light path at Mace Head, Ireland. Details on the instrument and the analysis procedure can be found in (from Allan et al., 2000, Copyright by American Geophysical Union (AGU), reproduced by permission of AGU)

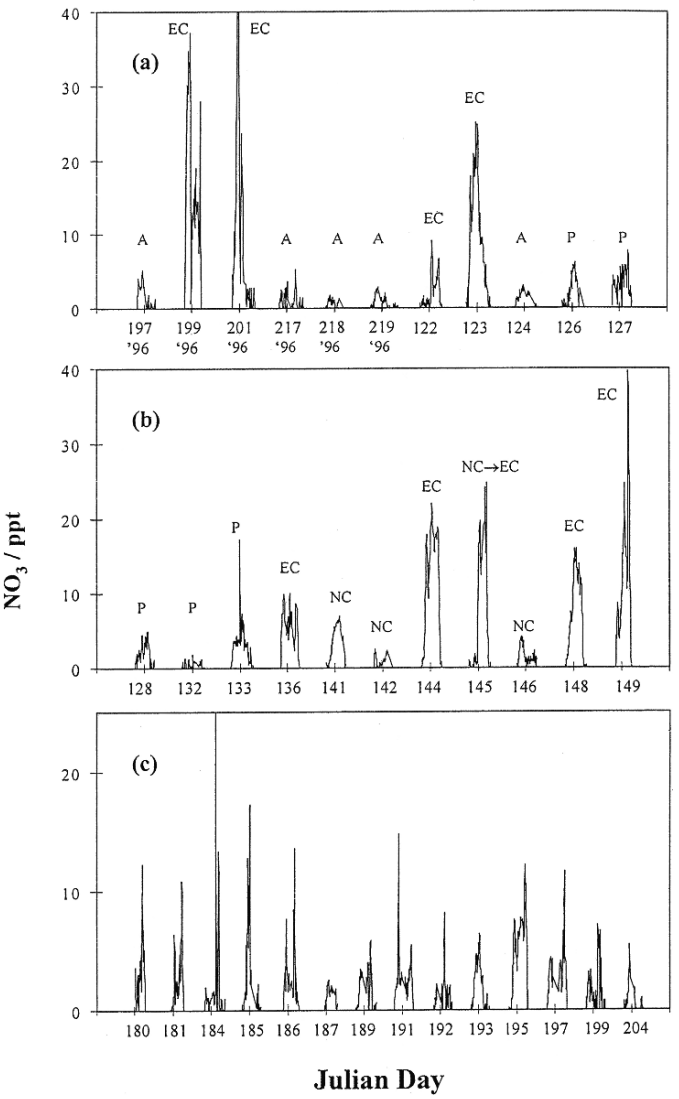

Fig. 10.28. NO_3 time series collected in the marine boundary layer of Mace Head, Ireland (**a** and **b**). The letters denote the origin of the observed air masses: A, atlantic; P, polar marine; EC, easterly continental; NC, northerly continental (from Allan et al., 2000, Copyright by American Geophysical Union (AGU), reproduced by permission of AGU)

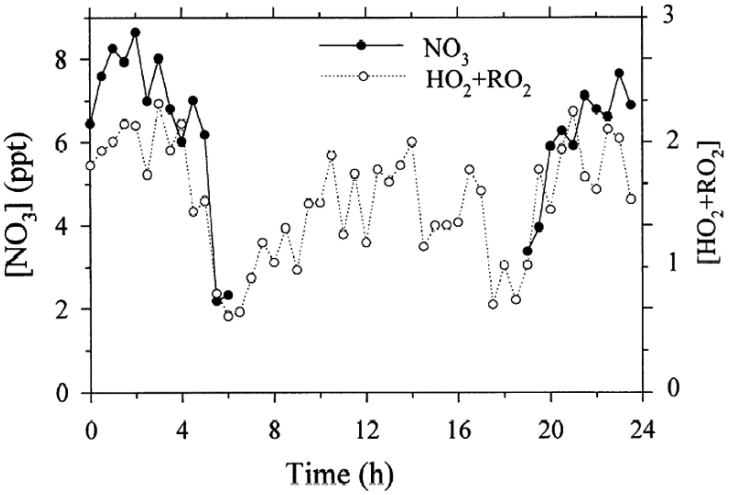

Fig. 10.29. Diurnal variation of NO_3 and $HO_2 + RO_2$ produced by averaging half-hourly data taken during 5 days (from Carslaw et al., 1997, Copyright by American Geophysical Union (AGU), reproduced by permission of AGU)

explained by the often high NO levels at the ground in cities, which efficiently destroy NO_3. As shown in Figs. 10.16 and 10.17, the levels of NO_3 are quite high in the upper nocturnal boundary layer. Mixing ratios above 100 ppt are frequently observed in cities, in which both precursors of NO_3, O_3, and NO_2, are elevated. Studies by Geyer and Stutz (Geyer et al., 2003; Stutz et al., 2004) showed that NO_3 can play an important role for the removal of NO_x and VOCs emitted by traffic in cities.

10.2.3 Measurement of Halogen Oxides

The discovery of boundary-layer ozone depletion events in the Arctic (Oltmans and Komhyr, 1986; Barrie et al., 1988; Bottenheim et al., 1990; Niki and Becker, 1993) has increased the interest in the chemistry of reactive halogens in the troposphere. DOAS measurements by Hausmann and Platt (1994) showed for the first time that these depletion events, during which ozone drops from ~ 40 ppb to unmeasurable levels (<2 ppb), are associated with high concentrations of reactive bromine, in particular BrO. Sources of gas phase Br are most likely heterogeneous reactions of oxides of nitrogen with sea-salt surfaces (Barrie et al., 1988; Finlayson-Pitts et al., 1990; Fan and Jacob 1992). Details of this chemistry are discussed in Chap. 2.

Here, we will present a number of examples of the measurement of halogen oxides and point out how these observations have advanced our understanding of halogen chemistry.

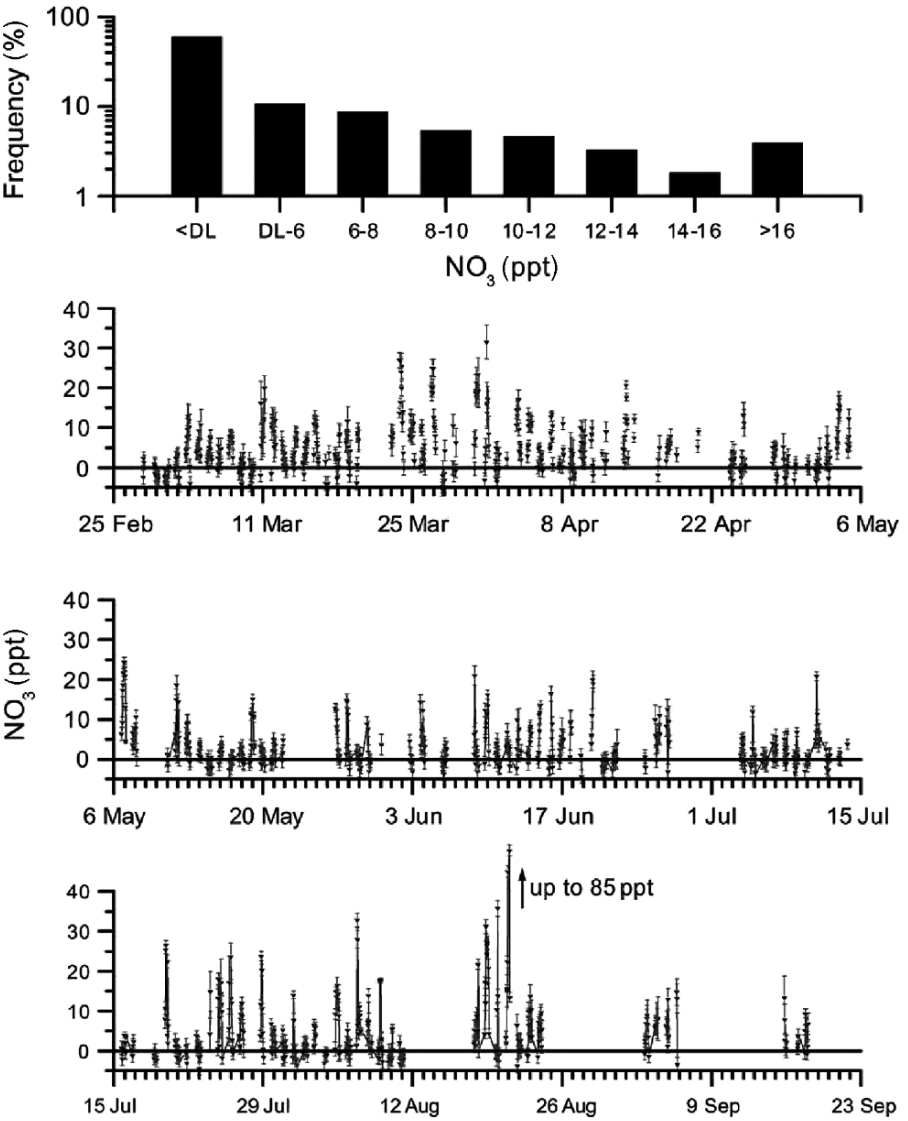

Fig. 10.30. Night-time NO_3 radical concentration profiles observed during a long-term campaign in a semi-rural area (Lindenberg near Berlin, Germany). Time series and frequency distribution (top panel, in 2-ppt intervals centred at the number given, DL = detection limit) of NO_3 observed by DOAS measurements averaged over a 10-km light path from February 27 to September 18, 1998. During the night from August 20–21, 1998, NO_3 reached peak mixing ratios up to 85 ppt. (from Geyer et al., 2001, Copyright Elsevier, 2001)

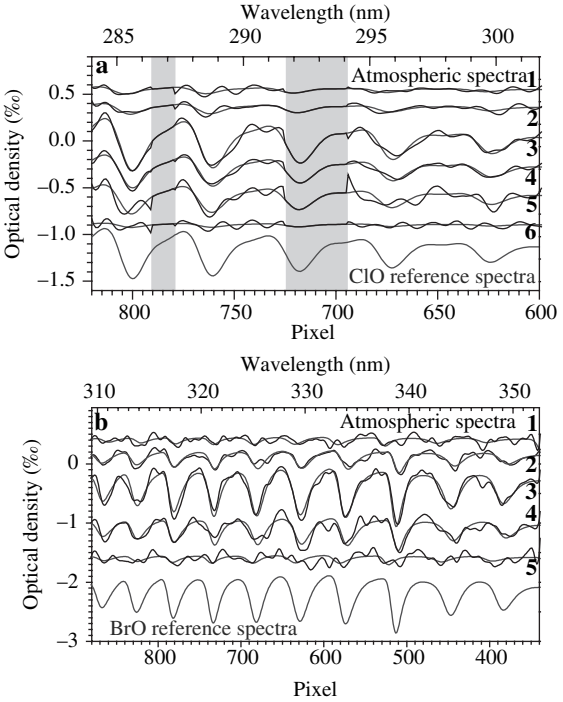

Fig. 10.31. ClO (**a**) and BrO (**b**) absorption structures recorded at the Great Salt Lake during October 14, 2000. The *black lines* are the atmospheric spectra after removing all absorptions except those by the respective halogen oxides. The *blue lines* are the respective fitted reference spectra that were calculated from a literature absorption cross-section (Orphal et al., in press; Sander and Friedl, 1989). Spectra are offset to each other to simplify the graph. The *grey intervals* in (a) mark spectral regions that were excluded from the fit (from Stutz et al., 2002b, Copyright by American Geophysical Union (AGU), reproduced by permission of AGU)

First, we show examples of the identification of the various halogen oxides in the atmosphere. Figures 10.31 and 10.35 show the spectra of ClO and BrO at the Great Salt Lake in Utah (Stutz et al., 2002). Similar examples for the detection of BrO can be found for the Dead Sea (Hebestreit et al., 1999) and polar regions (e.g. Hausmann and Platt, 1994; Tuckermann et al., 1997). The detection of ClO is more challenging due to the shorter wavelengths and the weaker absorptions.

Figures 10.32 and 10.33 show the identification of IO (Alicke et al., 1999) and OIO (Allan et al., 2001) in the atmosphere of Mace Head. Measurements of IO have been made at other locations and there is increasing evidence that IO is more ubiquitous than thus far assumed (Platt and Hönninger, 2003; Saiz-Lopez et al., 2004b; Zingler and Platt, 2005; Peters, 2004; Peters et al., 2005).

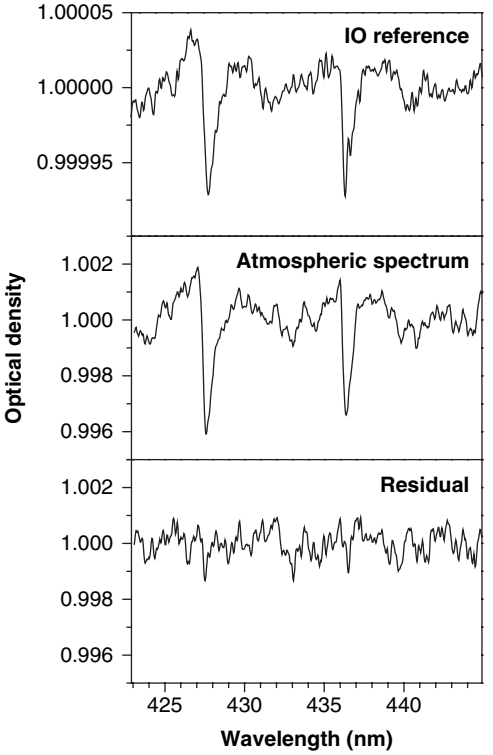

Fig. 10.32. Comparison of atmospheric spectrum after the removal of NO_2 and H_2O absorptions (centre panel) with the IO spectrum (top panel) clearly shows the presence of IO (from Alicke et al., 1999)

The study of the chemistry of BrO in polar regions was the first scientific application for the capability of DOAS to measure halogen oxides. Figure 10.34 shows data from a field experiment in Ny Alesund, Spitsbergen, during Spring 1996. The onset of ozone decay coincides with elevated BrO levels, providing evidence for the catalytic O_3 destruction cycles described in Chap. 2. The observation at the Dead Sea, Israel, (Fig. 10.35) confirm these results. The Dead Sea has the highest BrO levels thus far reported. With up to 100 ppt of BrO, the complete destruction of O_3 proceeds very fast and influences wide areas in the Dead Sea valley (Hebestreit et al., 1999; Matveev et al., 2001).

DOAS has provided evidence for the presence of four halogen oxides and is the most reliable method to measure these compounds today. Since tropospheric halogen chemistry is an active research field, DOAS will continue making contributions by providing accurate measurements of these species.

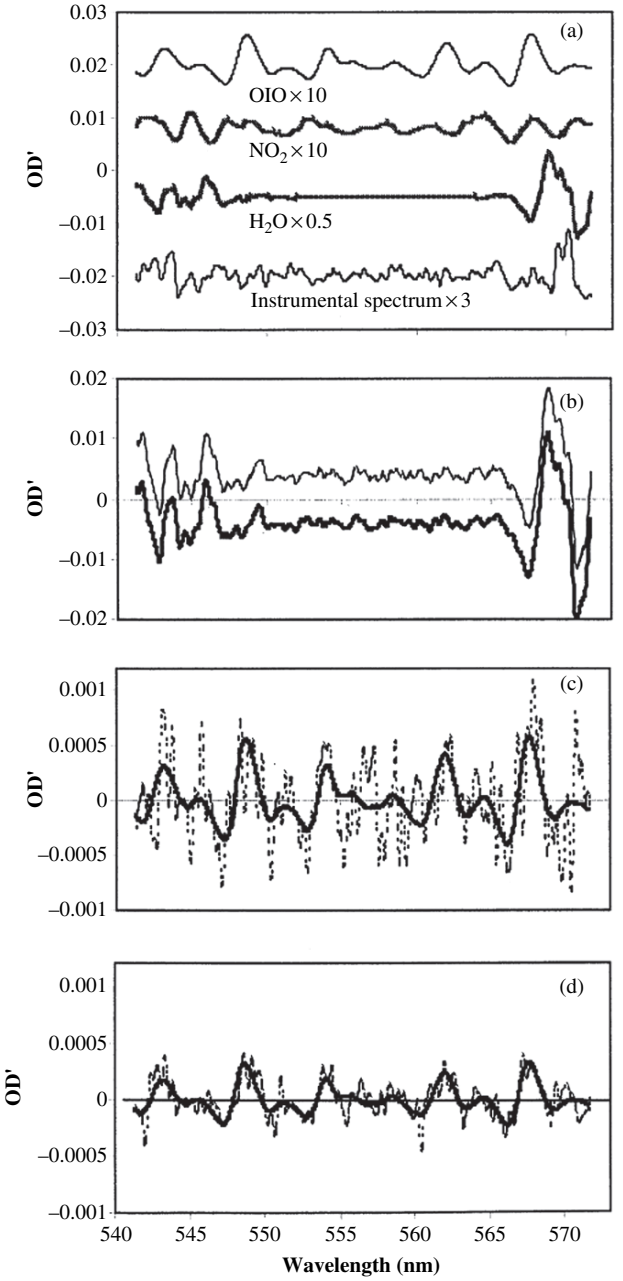

Fig. 10.33. OIO analysis from an atmospheric spectrum. *Panel* (**a**) shows the reference spectra used in the analysis; *Panel* (**b**) depicts the atmospheric spectrum containing all the absorbers. In *panel* (**c**) the absorptions of NO_2 and H2O have been removed. The OIO absorptions in this spectrum correspond to a mixing ratio of 1.8 ± 0.3 ppt. *Panel* (**d**) shows the residual of the analysis (from Allan et al., 2001, Copyright by American Geophysical Union (AGU), reproduced by permission of AGU)

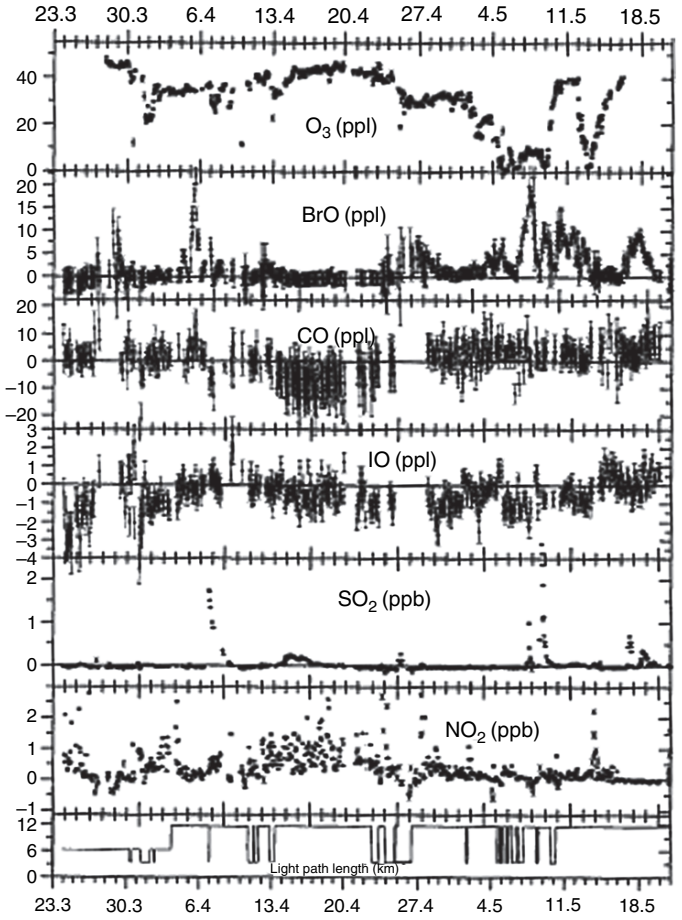

Fig. 10.34. DOAS measurements during Spring 1996 in Ny Alesung, Spitsbergen. The anti-correlation between BrO and O_3 can clearly be seen. Errors are 1σ uncertainties (adapted from Tuckermann 1996)

10.3 Investigation in Photoreactors (Smog Chambers) by DOAS

Since its development in the late-1970s DOAS has also been used in aerosol and smog chambers. To our knowledge the first measurements were made in Riverside in 1979 to investigate the formation of nitrous acid.

More recently, comprehensive DOAS measurements were performed in the EUROpean PHOto REactor (EUPHORE) in Valencia, Spain (Becker, 1996). The set-up is shown in Fig. 10.37. In particular, kinetic and mechanistic studies of the degradation of monocyclic aromatic species were followed by DOAS (Volkamer, 2001; Volkamer et al., 2001, 2002). A sample time series

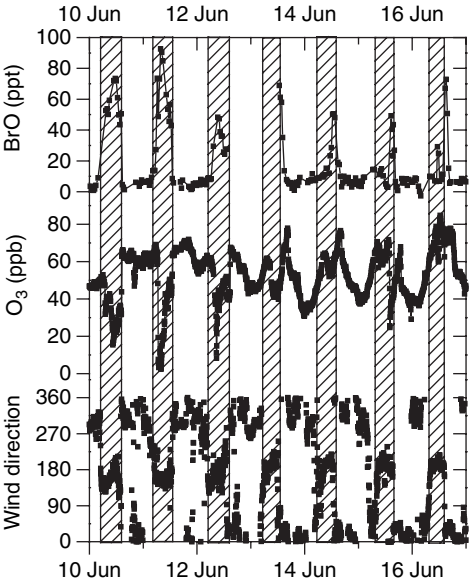

Fig. 10.35. DOAS measurements at the Dead Sea, Israel. The regular pattern in O_3 and BrO is caused by the changing wind direction and the chemical destruction of ozone (from Hebestreit et al., 1999)

of photochemical p-xylene degradation and corresponding formation of the degradation products p-tolualdehyde, 2,5-dimethylphenol, and glyoxal – all measured by DOAS – is shown in Fig. 10.38.

10.4 Validation of Active DOAS

An important aspect for all measurement techniques is the determination of the observational accuracy. In particular, for measurements in the open atmosphere only one method is available to determine the accuracy of a measurement, the comparison of different analytical techniques. The statistical approach, i.e. repeating a measurement several times, is not available due to the ever changing conditions in the atmosphere.

As described in Chap. 6, DOAS is an absolute analytical method. Calibrations are not needed and the accuracy is determined by the accuracy of the absorption cross-sections used in the analysis of the DOAS spectra. However, as in all analytical techniques, the possibility of unknown systematic errors always has to be considered. An intercomparison between DOAS and other techniques is thus a valuable exercise. Often intercomparisons between DOAS and other techniques are used for the benefit of the other techniques which may have calibration problems, for example OH-LIF systems.

Shown here are a number of examples for intercomparisons for the most important trace gases. Measurements of O_3 and SO_2 were made by a long-path

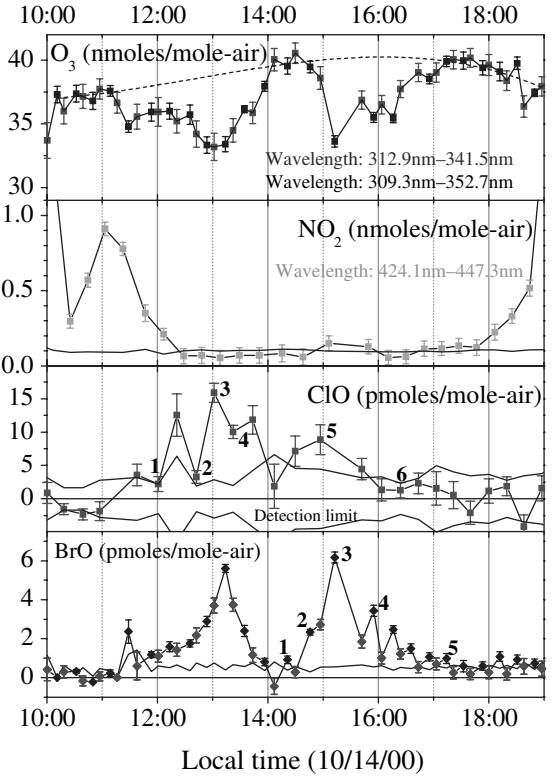

Fig. 10.36. Mixing ratios of O_3, NO_2, BrO, and ClO measured at ground level on October 14, 2000. The different symbols in the ozone and BrO traces indicate the different grating position used in the measurements. The *solid brown lines* show the detection limit determined for each individual spectrum (from Stutz et al., 2002, Copyright by American Geophysical Union (AGU), reproduced by permission of AGU)

DOAS instrument, a UV ozone monitor, and a commercial SO_2 monitor at the University of East Anglia Atmospheric Observatory at Weybourne, England (Stutz, 1996). Weybourne is located at the East coast of England, in an area with few pollution sources. The observed air masses were thus fairly well mixed, facilitating the comparison of the in situ technique with the DOAS data which were averaged over a 3.5-km-long light path. Figure 10.39 shows the excellent agreement between the methods. The difference between the DOAS and the in situ O_3 measurement is $\sim 5\%$, which is in the range of the accuracy of both the methods. While the slope of the SO_2 correlation is 1.01, the data is considerably more scattered than that of O_3. This is mainly caused by localised SO_2 sources close to the observatory, for example ships cruising off the coast. In both cases, small offsets were found. The reason for these offsets is unclear.

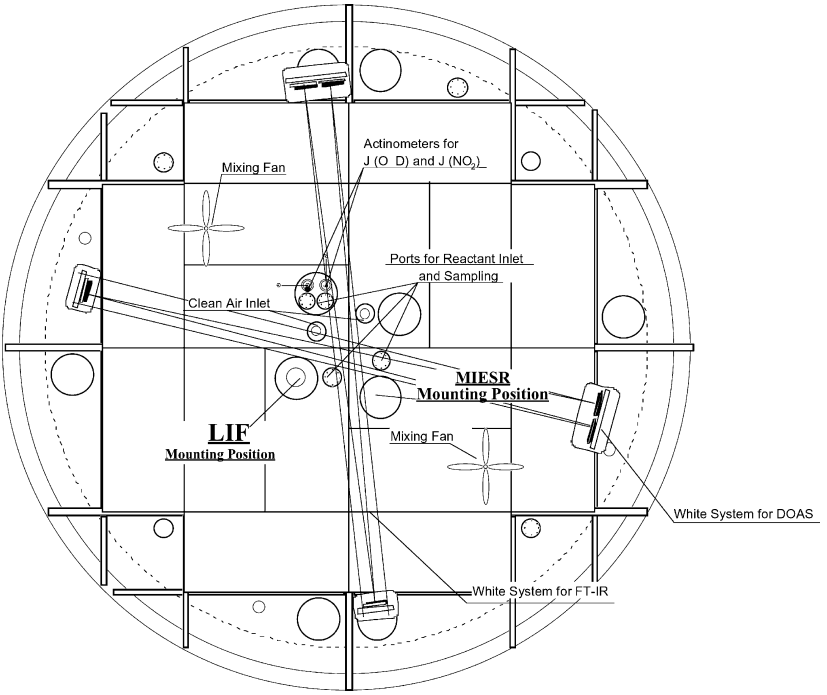

Fig. 10.37. Schematic of the DOAS multi-reflection system (White system) in the EUPHORE chamber in Valencia, Spain (from Volkamer et al., 2002, reproduced by permission of the PCCP Owner Societies)

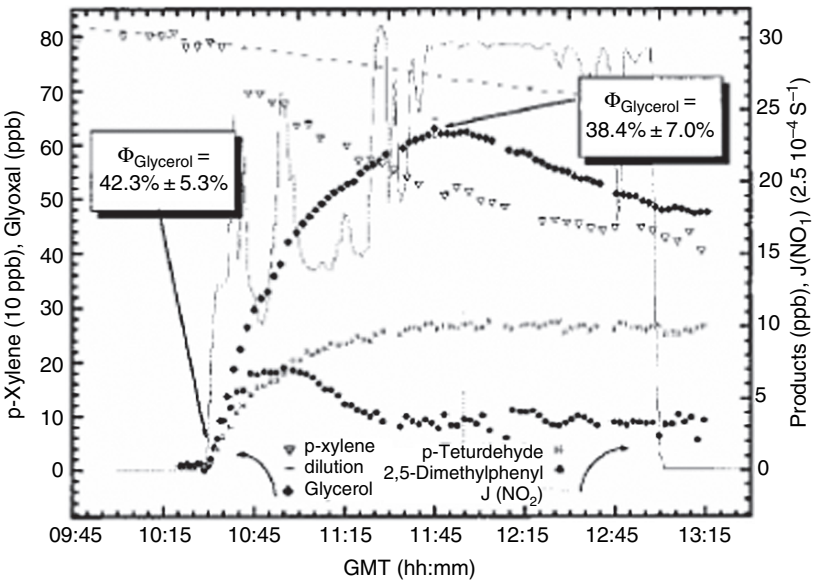

Fig. 10.38. Concentration time profile of various aromatic hydrocarbons during the oxidation of p-xylene (from Volkamer et al., 2002, reproduced by permission of the PCCP Owner Societies)

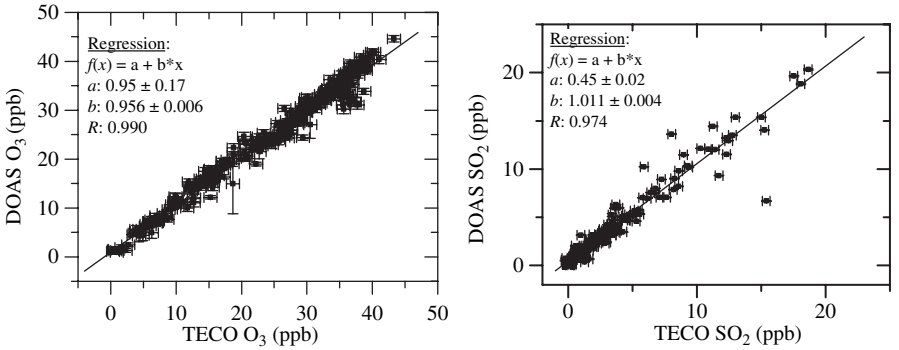

Fig. 10.39. Intercomparison between in situ O_3 and SO_2 instrument and a long-path DOAS system in Weybourne, England (from Stutz, 1996)

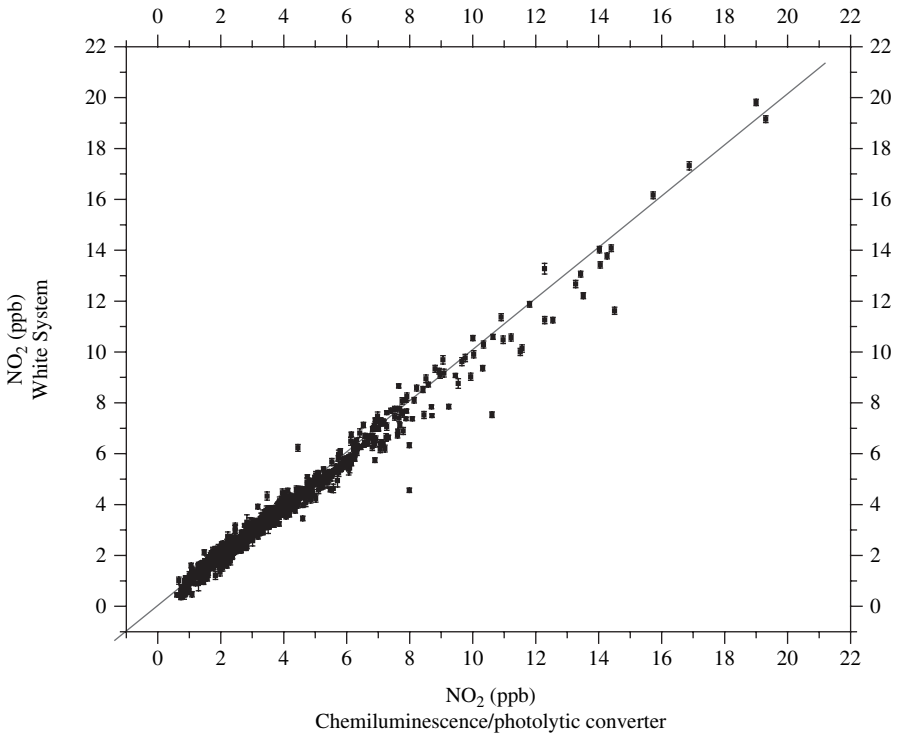

Fig. 10.40. Intercomparison of a multi-reflection DOAS instrument and an in situ NO_2 monitor. Both instruments were set up side-by-side at an altitude of 8 m above the ground on a meadow 50 km southeast of Berlin, Germany, during the BERLIOZ experiment (from Alicke et al., 2003, Copyright by American Geophysical Union (AGU), reproduced by permission of AGU)

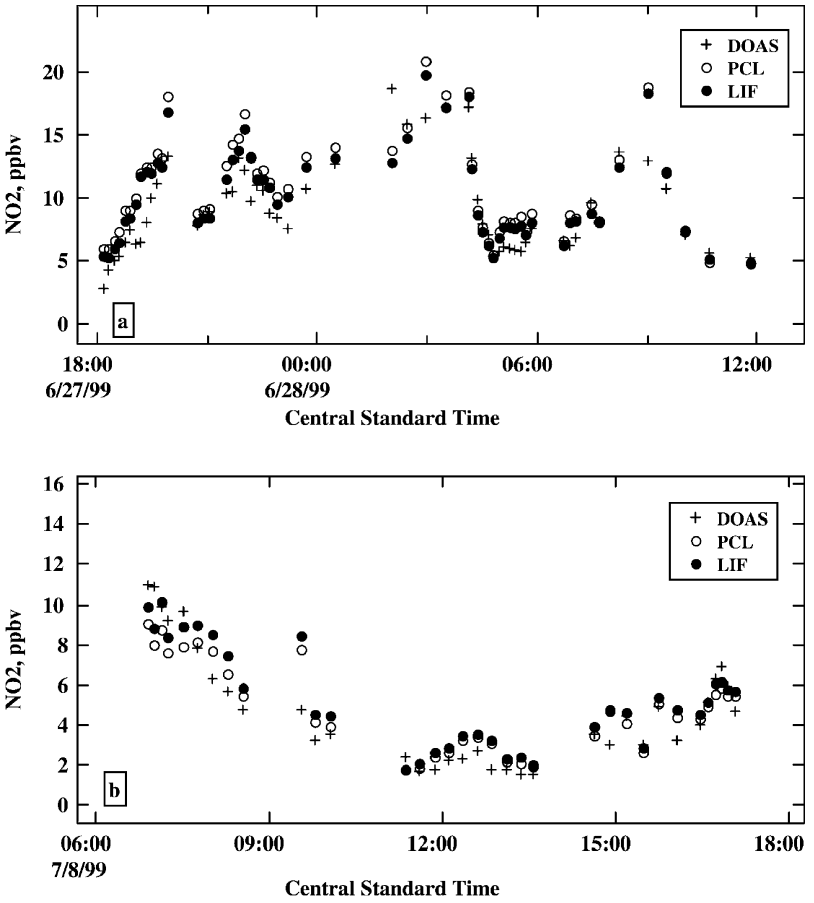

Fig. 10.41. Comparison of three NO_2 measurement methods: DOAS, Photolytic Converter/chemoluminescence, PCL, and Laser Induced Fluorescence, LIF (from Thornton et al. 2000); during the Southern Oxidant Study (SOS) 1999, in Nashville, TN, USA. The measurement was performed in a shallow river valley. The DOAS light beam crossed the entire extent (vertical and horizontal) of the valley, while the in situ instruments sampled 10 m above the ground (from Thornton et al., 2003, Copyright by American Geophysical Union (AGU), reproduced by permission of AGU)

Figure 10.40 shows the intercomparison of a multi-reflection DOAS system with 15m base path length and a NO_2 in situ instrument based on the photolytic conversion of NO_2 to NO followed by the detection of NO through chemoluminescence (Alicke et al., 2003). This intercomparison was performed during the BERLIOZ campaign in 1998, $\sim$ 50 km southeast of the city centre of Berlin, Germany. A linear regression weighted by the error of the DOAS system yields a slope of 1.006 ± 0.005 (White system against chemoluminescence system). The

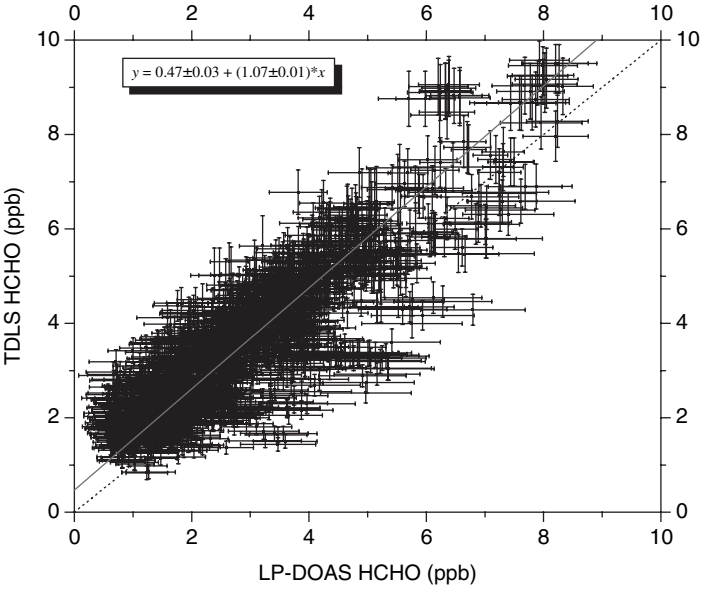

Fig. 10.42. Intercomparison of simultaneous formaldehyde measurements by a Tuneable Diode Laser Spectrometer (TDLS) in situ instrument and a long-path DOAS system during the Southern Oxidant Study (SOS), 1999 in Nashville, TN, USA. Shown is the entire dataset during 4 weeks of this experiment. (TDLS HCHO data courtesy of A. Fried, NCAR)

intercept of (36 ± 19) ppt is statistically insignificant. The excellent agreement between the two methods shows the accuracy of both methods.

Another intercomparison between three different methods is shown in Fig. 10.41 (Thornton et al., 2003). Here, a long-path DOAS instrument (path-length 2×1.35 km) was compared with two co-located point measurements by a Photolytic Converter/chemoluminescence instrument (PCL), and a laser induced fluorescence (LIF) system. The comparison shows that, in many situations, the agreement between the two in-situ instruments is better than with the DOAS instrument. This apparent disagreement is caused by the spatial averaging of the DOAS system. While an in situ instrument observes only a small air volume, the DOAS data represent an average over an extended air mass.

Under certain meteorological conditions, this can lead to a disagreement between DOAS and other methods. Whenever data from a long-path DOAS instrument is used, this averaging has to be considered. An example for this effect can also be observed in Fig. 10.16, where the spatial inhomogeneity of certain trace gases is illustrated.

During the same field experiment, intercomparison between a TDLS HCHO instrument (Fried A, personal communication) and the long-path DOAS was performed. While the statistical errors of both the methods were $\sim$ 0.2–0.5 ppb, Fig. 10.42 shows an excellent agreement between the two

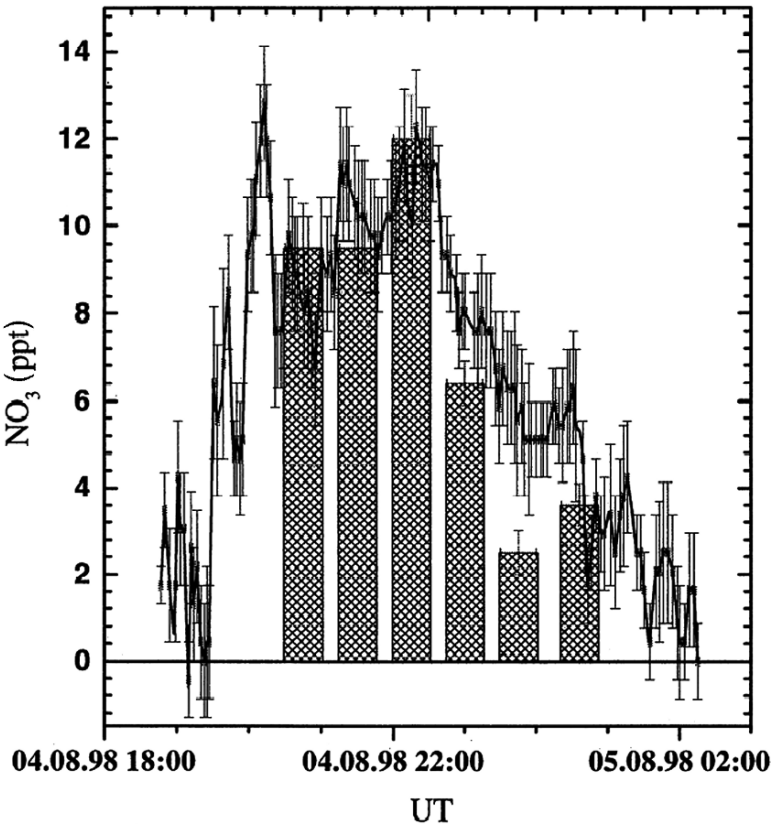

Fig. 10.43. Observation performed by a long-path DOAS instrument (*line*) and a matrix isolation electron spin resonance method (*bars*) during the BERLIOZ experiment, near Berlin, Germany (from Geyer et al., 1999, Copyright by American Geophysical Union (AGU), reproduced by permission of AGU)

methods. The slope of 1.07 ± 0.01 is within the range of the accuracy of both instruments.

The various intercomparisons show the accuracy of DOAS when compared with other methods. In general, the agreement is within the accuracies determined by the different absorption cross-sections. However, spatial inhomogenities can have a considerable influence on the quality of the intercomparisons.

While many intercomparisons for pollutants have been made, few examples exist for radical species. Geyer et al. (1999), showed a comparison between a long-path DOAS instrument and a matrix isolation electron spin resonance (MIESR) method. These measurements were performed during the BERLIOZ experiment in 1998. The authors also included data from an older field experiment in Deuselbach, Germany in 1983. The comparison of the

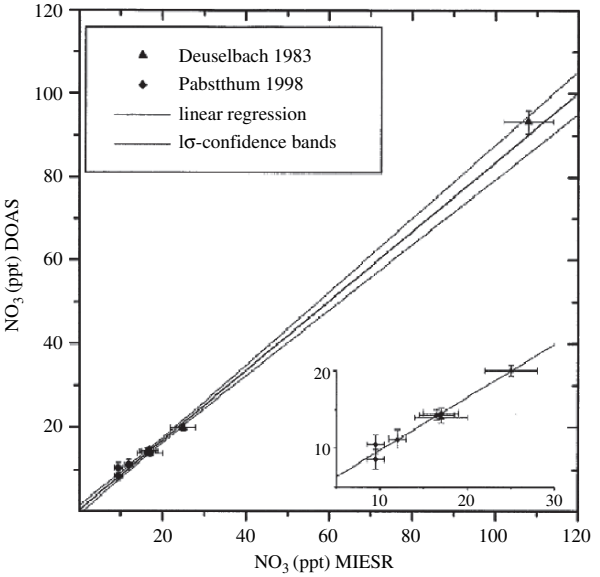

Fig. 10.44. Correlation between DOAS and MIESR measurements from two field experiments. Data marked with *triangles* were measured in Deuselbach in May/June 1983, while data denoted by *diamonds* were obtained during BERLIOZ in summer 1998 (from Geyer et al., 1999, Copyright by American Geophysical Union (AGU), reproduced by permission of AGU)

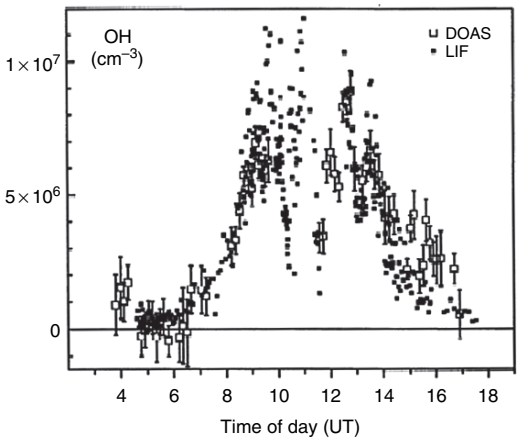

Fig. 10.45. Intercomparison of OH measurements by a multi-reflection DOAS system and a laser-induced fluorescence instrument (from Brauers et al., 1996, Copyright by American Geophysical Union (AGU), reproduced by permission of AGU)

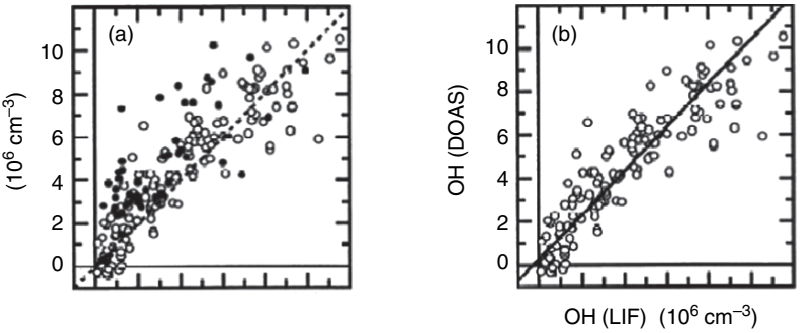

Fig. 10.46. Correlation of DOAS and laser-induced fluorescence data. *Panel* (a) shows the entire dataset for 11 days in August 1994, while *Panel* (b) presents a reduced dataset, where data from a windsector from 285–20 was excluded. The correlation coefficient was 0.9. The *solid line* represent the weighted linear fit given by $[\mathrm{OH}]_{\mathrm{DOAS}} = (1.01 \pm 0.04) \times [\mathrm{OH}]_{\mathrm{LIF}} + (0.28 \pm 0.15)$ (from Brauers et al., 1996, Copyright by American Geophysical Union (AGU), reproduced by permission of AGU)

measured data (Fig. 10.43) shows an excellent agreement, in particular considering that the DOAS are measured over a 3.5-km-long path while the MIESR data were sampled at one point. In addition, the MIESR data are averaged over 1 h, while the DOAS time resolution was ~ 5 min.

The correlation plot of the BERLIOZ and Deuselbach data also illustrates the excellent agreement between the two methods (Fig. 10.44). It is remarkable

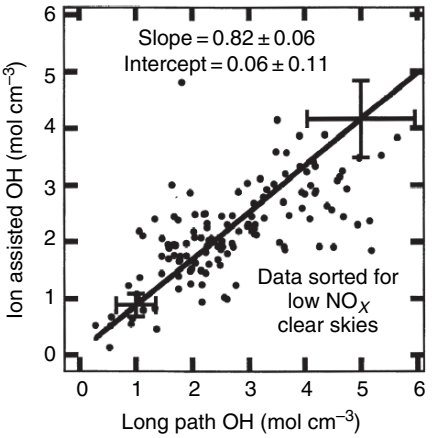

Fig. 10.47. Intercomparison of OH measurements by a long-path DOAS system and a chemical ionisation mass spectrometer in the mountains near Boulder, CO (Mount et al., 1997). Only data from clear days with $\mathrm{NO_X}$ levels below 500 ppt are shown (from Mount et al., 1997, Copyright by American Geophysical Union (AGU), reproduced by permission of AGU)

that this agreement is achieved using two datasets that were acquired 15 years apart.

The study by Geyer et al. (1999) leaves little doubt about the accuracy of both DOAS and MIESR data.

One of the most challenging measurements is that of the OH radical. Because of its high reactivity and low concentrations, atmospheric measurements typically have large uncertainties. It is thus essential to compare different analytical methods of this elusive radical to assess how well we can determine atmospheric OH concentration. Brauers et al. (1996) showed one of the first intercomparisons between a DOAS and a LIF instrument. The DOAS instrument was based on a multi-reflection system with 20 m base path length (see also above). Figure 10.45 shows the comparison between the data of both instruments during a diurnal cycle. The agreement is quite good, as can also be seen in the correlation of data over an 11-day period (Fig. 10.46).

Mount et al. (1997), showed a similar OH comparison between a long-path DOAS instrument and a chemical ionisation mass spectrometer, confirming the accuracy of the measurements (Fig. 10.47).